magnetochemistry

MDPI

Review

Magnetoelectric Core–Shell Nanoparticles for Biomedical and Bioelectronic Applications: Materials, Transduction Mechanisms, Surface Engineering, and Translational Perspectives

Selcuk Atalay

Department of Physics, Inonu University, 44280 Malatya, Turkey; selcuk.atalay@inonu.edu.tr

Abstract

Magnetoelectric materials couple magnetic and electrical order parameters and can convert remotely applied magnetic fields into localized electrical responses. At the nanoscale, this functionality is commonly pursued through core–shell architectures in which a magnetostrictive or magnetic core is mechanically coupled to a piezoelectric or ferroelectric shell. The resulting strain-mediated transduction is attractive for biomedical and bioelectronic applications because magnetic fields penetrate biological tissue with comparatively low attenuation, whereas the generated electrical signals can interact directly with charged biomolecules, cell membranes, ion channels, and electroactive tissues. This review critically evaluates magnetoelectric core–shell nanoparticles from a broad biomedical and bioelectronic perspective. The physical basis of direct and converse magnetoelectric coupling is first discussed, with emphasis on nanoscale boundary conditions, magnetic-domain state, ferroelectric polarization, interfacial strain transfer, ionic screening, and nonlinear field dependence. Representative magnetic-core/piezoelectric-shell material families, including ferrite-based, multiferroic-oxide, lead-free piezoelectric, PZT-containing, and polymer-integrated architectures, are compared in terms of magnetic response, piezoelectric activity, chemical stability, biocompatibility, toxicity, and processability. Particular attention is given to $CoFe_2O_4$–$BaTiO_3$ (CFO-BTO) as a benchmark magnetoelectric core–shell system, while alternative material combinations are comparatively discussed to reflect the broader diversity of the field. Synthesis and processing strategies, structural and physicochemical characterization, surface engineering, and local or macroscopic magnetoelectric measurement methods are examined together with the artifacts that can complicate quantitative interpretation. Particular attention is paid to particle size, shell thickness, crystallinity, aggregation, colloidal stability, surface chemistry, biomolecular functionalization, and their influence on magnetoelectric performance and biological interactions. The available literature demonstrates substantial progress in magnetically triggered drug delivery and cancer therapy, wireless neural and cardiac stimulation, tissue engineering, immunomodulation, wound healing, multimodal imaging, and related bioelectronic applications. Biosensing is also considered an important emerging direction; however, direct quantitative detection of proteins, nucleic acids, pathogens, and cancer biomarkers using isolated core–shell magnetoelectric nanoparticles remains comparatively underdeveloped. The review therefore distinguishes experimentally established biomedical and bioelectronic functionalities from less mature biosensing concepts and identifies the measurement, safety, clinically relevant magnetic-field exposure, scalable manufacturing, device-integration, and regulatory challenges that must be addressed for translation. A practical roadmap is proposed for developing reproducible, lead-free, biologically stable, and quantitatively characterized magnetoelectric nanoparticle platforms for next-generation wireless biomedical and bioelectronic technologies.

Check for updates

Academic Editors: Wei Zhang and Xiaogang Yu

Received: 3 August 2026
Revised: 25 August 2026
Accepted: 14 September 2026
Published: 16 September 2026

Copyright: © 2026 by the author. Licensee MDPI, Basel, Switzerland. This article is an open access article distributed under the terms and conditions of the Creative Commons Attribution (CC BY) license.

Keywords: magnetoelectric nanoparticles; core–shell nanostructures; biosensors; magnetoelectric coupling; surface functionalization; neural stimulation; targeted drug delivery; biocompatibility; wireless bioelectronics

1. Introduction

Magnetoelectric (ME) materials provide a direct physical bridge between magnetic and electrical variables. In a direct ME process, a magnetic stimulus produces an electrical response; in the converse process, an electric field changes magnetization or a related magnetic state. Single-phase multiferroics can display both magnetic and ferroelectric order, but their room-temperature coupling is often too weak, too lossy, or too difficult to engineer for biomedical use. Multiphase composites therefore dominate practical ME research because magnetostriction in one phase can be mechanically transferred to a piezoelectric phase, producing polarization or voltage without requiring a large current at the point of action. Core–shell nanoparticles represent the nanoscale limit of this composite concept and maximize interfacial area while enabling dispersion in liquids, incorporation into polymers or hydrogels, and localization near biological targets [1]. Historically, the renewed interest in composite magnetoelectrics arose from the limitations of single-phase multiferroics. Although magnetoelectricity was recognized experimentally decades ago, many single-phase compounds combine weak room-temperature coupling with low magnetic ordering temperatures, leakage, or difficult processing.

Multiphase composites circumvent these limitations by assigning magnetic-field-to-strain conversion and strain-to-charge conversion to separate phases. This strain-mediated strategy underpins layered magnetoelectric devices [2–4] and was later extended to dispersed core–shell nanostructures with a much larger interfacial area-to-volume ratio [1]. The biomedical significance of this transition is not simply miniaturization. Conventional electrodes deliver electrical stimulation along a conductive path and may affect tissue outside the intended target. A dispersed or locally immobilized magnetoelectric transducer instead offers the possibility of producing electrical cues near a selected cell population under external magnetic control. The practical objective is therefore spatially confined, wireless stimulation or sensing at nano-to-microscale dimensions, while avoiding the power leads, rigid electrodes, and line-of-sight restrictions associated with conventional bioelectronic interfaces [3]. The biomedical motivation is compelling. Magnetic fields can be produced outside the body and can penetrate soft tissue without the line-of-sight requirement of optical stimulation.

A magnetostrictive core can convert that field into strain, while a piezoelectric shell can convert the strain into surface charge or a local electric field. In principle, the same particle can act as a remotely powered transducer, a magnetic imaging label, a drug carrier, and a nanoscale electrode. This combination has led to the broader view of magnetoelectric nanoparticles (MENPs) as enabling components for "technobiology", in which information and energy are exchanged between engineered nanomaterials and biological systems [5]. The concept is especially attractive for neural interfaces, where conventional electrodes require implantation and wired power, but it is also relevant to tumor targeting, controlled drug release, tissue regeneration, inflammation control, cardiac stimulation, and biosensing. The term "core–shell", however, is used inconsistently in the literature. In this review, a true core–shell MENP is defined as a discrete nanoscale particle in which one functional phase forms an identifiable core and the second forms a continuous surrounding shell; conventional magnetic-core/piezoelectric-shell and inverse core–shell variants are both included when this morphology is experimentally supported (Figure 1). Systems in

which a verified core–shell nanoparticle is further coated with a continuous functional or biological layer, or embedded within a polymer, hydrogel, scaffold, or other hierarchical host, are classified as core–shell-derived systems. By contrast, 0–3 particle–polymer composites, electrospun fibers without a discrete core–shell nanoparticle unit, thin films, laminates, resonators, antennas, and larger magnetoelectric devices are classified as related ME composites/devices. These categories are used consistently throughout the review, and cross-architecture comparisons are made only to extract transferable design principles rather than to imply structural equivalence.

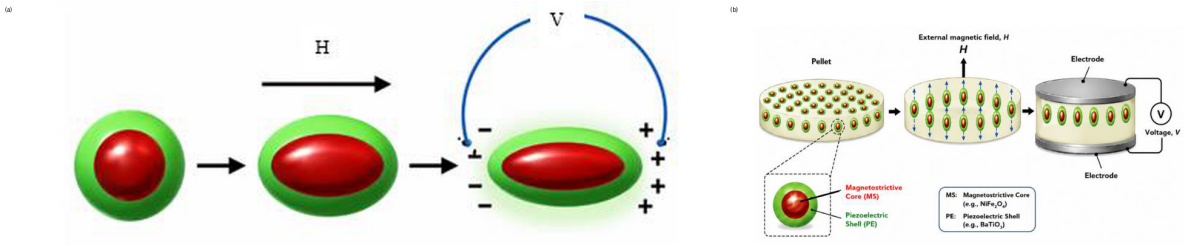


Figure 1. Schematic illustration of magnetoelectric voltage generation at the single-particle and pellet levels: (**a**) deformation and electrical polarization of an individual magnetostrictive-core-piezoelectric-shell nanoparticle under an external magnetic field and (**b**) collective voltage generation in a compacted pellet composed of core–shell magnetoelectric nanoparticles. The magnetic-field-induced deformation of the magnetostrictive cores is transferred to the piezoelectric shells, producing polarization changes that are detected as a voltage across electrodes deposited on the opposing pellet surfaces.

A further challenge is that the evidence base is uneven. Materials studies often report X-ray diffraction, electron microscopy, magnetic hysteresis, and piezoresponse measurements, whereas biomedical papers may demonstrate cellular effects without directly quantifying the local electric field or ME coefficient under the exact biological exposure conditions. Conversely, some exceptionally high nanoscale ME coefficients have been reported using single-particle probes, but these values are difficult to compare with macroscopic powder-compaction or polymer-composite measurements. The field thus needs a common language linking material composition, particle architecture, measurement geometry, magnetic excitation, electrical readout, and biological outcome. This review addresses that need through a biomedical and bioelectronic framework that maintains explicit separation among true core–shell MENPs, core–shell-derived systems, and related ME composites/devices.

It first describes the physical basis of nanoscale strain-mediated coupling and then compares magnetic cores, piezoelectric shells, and hybrid matrices. Synthesis, structural characterization, local electrical measurements, and magnetoelectric testing are evaluated with emphasis on reproducibility and artifacts. The review next analyzes structure–property relationships, surface functionalization, colloidal behavior, and biological interfaces. Biosensing principles are evaluated alongside, but separately from, broader therapeutic and bioelectronic applications so that the maturity and evidence level of each use case can be assessed. Finally, biocompatibility, field safety, manufacturing, device integration, and regulatory translation are considered. The central argument is that MENPs have become credible wireless transducers for selected biomedical and bioelectronic applications, particularly neuromodulation and field-controlled therapeutic delivery, whereas quantitative biosensing remains less mature and requires more standardized transduction measurements, target-recognition chemistry, calibration models, and in vivo validation.

The literature considered in this review was identified through searches of the Web of Science and Scopus databases using combinations of keywords related to the main

scope of the article, including "magnetoelectric nanoparticles," "magnetoelectric core–shell nanoparticles," "magnetoelectric nanocomposites," "magnetoelectric coupling," "biomedical applications," "bioelectronics," "biosensing," "drug delivery," "neuromodulation," and "tissue engineering." No predefined publication-date restriction was applied; the final cited literature spans approximately 2005–2026, thereby incorporating both foundational studies and recent developments. Publications were selected primarily on the basis of their direct relevance to magnetoelectric core–shell or closely related nanoparticle architectures, materials design and synthesis, magnetoelectric transduction and characterization, surface engineering, biomedical or bioelectronic applications, and biological safety. Peer-reviewed experimental, mechanistic, and application-oriented studies were prioritized, while broader nanoparticle or device literature was included selectively when it provided transferable context for surface functionalization, drug delivery, sensing, safety, or device integration.

2. Fundamentals, Materials, and Structure–Property Design

2.1. Magnetoelectric Coupling and Nanoscale Operating Regime

The direct ME effect describes the generation of electric polarization, charge, or voltage in response to a magnetic field. In a strain-mediated core–shell particle, the applied field changes the dimensions of the magnetic phase through magnetostriction. The resulting stress is transmitted across the interface to the piezoelectric shell, where it changes polarization. The converse ME effect follows the reverse sequence: an electric field strains the piezoelectric phase and thereby modifies magnetic anisotropy, magnetization, coercivity, or domain structure in the magnetic phase. For biomedical stimulation, the direct mode is usually emphasized because an externally applied magnetic field is converted into a local electrical cue. For active sensing or bidirectional neural interfaces, the converse mode is also important because a biological electric potential could, in principle, modulate the particle magnetization and be detected remotely.

Figure 1 illustrates the magnetoelectric voltage-generation mechanism at both the single-particle and pellet levels. As shown in Figure 1a, each core–shell magnetoelectric nanoparticle consists of a magnetostrictive magnetic core mechanically coupled to a piezoelectric or ferroelectric shell. When an external magnetic field, H, is applied, the magnetostrictive core undergoes a field-induced dimensional change. This deformation is mechanically transferred to the surrounding shell, generating stress-induced polarization and charge redistribution within the piezoelectric phase. Consequently, a potential difference develops across the nanoparticle. In a compacted pellet containing many core–shell nanoparticles (Figure 1b), the electrical responses generated by the individual particles are collected through electrodes deposited on the opposing pellet surfaces and measured as an output voltage. The measured pellet voltage represents the collective magnetoelectric response of the nanoparticle ensemble and depends on particle orientation, interfacial strain transfer, porosity, electrical connectivity, magnetic-field amplitude and frequency, and the applied DC bias field. Therefore, the measured signal should be regarded as an orientation-and connectivity-weighted collective response rather than a simple arithmetic sum of identical single-particle voltages.

The magnitude of the response is often summarized by a voltage coefficient, $\alpha_E = \partial E/\partial H$, or by a charge, polarization, or surface-potential change per unit magnetic field. A heuristic scaling relation for a mechanically coupled two-phase particle is:

$$\alpha_E \approx \eta\, q_m\, d_p/(\varepsilon_0\, \varepsilon_r\, s_{eff}) \quad (1)$$

where η is an interfacial strain-transfer factor, $q_m = \partial\lambda/\partial H$ is the piezomagnetic coefficient of the core, d_p is an effective piezoelectric coefficient of the shell, $\varepsilon_0\varepsilon_r$ is its permittiv-

ity, and s_{eff} represents the effective elastic compliance of the coupled structure. This expression is not a universal solution for a spherical particle; it simply emphasizes that strong magnetostriction alone is insufficient. Efficient coupling also requires a large field derivative of magnetostriction, favorable elastic matching, low dielectric leakage, an active piezoelectric phase, and a mechanically coherent interface. Single-particle nanoprobe measurements reported ME coefficients above 5 V cm^{-1} Oe^{-1} for approximately 20 nm CFO-BTO particles and above 2 V cm^{-1} Oe^{-1} for $NiFe_2O_4$–$BaTiO_3$ particles [6]. These values were substantially larger than many conventional 0–3 composite values and were attributed to a lattice-matched interface and reduced charge leakage in a local probe geometry. The result established the possibility of very strong nanoscale coupling, but it also highlighted a persistent comparability problem: a local electric-field coefficient inferred at one nanoparticle is not equivalent to a voltage measured across a pellet, a polymer film, or a biological medium.

The magnetic core determines how effectively magnetic energy is converted into mechanical deformation. Cobalt ferrite is widely used because it combines chemical stability, high anisotropy, and appreciable magnetostriction. Magnetite and other iron oxides generally offer better-established biomedical compatibility but lower magnetostriction. Nickel ferrite can provide lower coercivity and a different frequency response, although small particles may become superparamagnetic and lose the quasi-static hysteretic response needed for strong low-frequency strain generation. Studies of iron oxide nanoparticle–$BaTiO_3$ composites demonstrate that electric-field control and ME coupling depend strongly on particle ordering, clamping, and core size [7]. More recent Fe_3O_4-$BaTiO_3$ work has shown that the magnetostriction coefficient and magnetic remanence increase with core size, while the smallest cores may be nearly superparamagnetic [8]. A useful design variable is not merely the saturation magnetostriction λ_s but the slope $q_m = \partial\lambda/\partial H$ in the operating field range. A highly magnetostrictive core that requires a very large bias field may be unsuitable for portable biomedical excitation.

Conversely, a softer magnetic core can provide a large small-signal response at low field even if its saturation magnetostriction is moderate. Recent local measurements on CFO-BTO agglomerates used magnetic-field-assisted piezoresponse force microscopy and Kelvin probe force microscopy to detect magnetic-field-induced phase and surface-potential changes [9]. Such studies reinforce the need to report the complete field waveform, amplitude, frequency, bias, particle orientation, and magnetic history. The operating-point concept is readily understood from macroscopic laminate measurements. For a piezoelectric layer of thickness t, the commonly reported voltage coefficient is $\alpha_E = V/(H_{AC}.t)$, where V is the induced voltage and H_{AC} is the amplitude of the alternating magnetic field. This definition is useful for devices and compacted composites, but it should not be transferred uncritically to isolated nanoparticles because the effective electrical path length, boundary conditions, and field distribution are different. Nevertheless, laminate studies remain valuable for defining the excitation and calibration principles used in nanoparticle measurements [10,11]. These laminate structures are treated here as related ME devices rather than core–shell MENPs; they are cited only for transferable bias-field, excitation, and calibration principles.

At zero DC bias, a small AC field may probe a region where the magnetostriction curve has a low slope and consequently generate only a weak electrical response. Applying an appropriate DC field shifts the operating point toward the region of maximum $d\lambda/dH$, allowing a larger small-signal response at the same H_{AC}. This is why the bias field, rather than only the saturation magnetostriction, must be reported and optimized. For biomedical systems, low-field materials are particularly desirable because producing spatially homogeneous kilooersted AC fields is technically difficult and may impose additional

heating and safety constraints [2,11]. At the nanoscale, thermal fluctuations compete with magnetic anisotropy. When the magnetic anisotropy energy approaches thermal energy k_BT, the magnetization can fluctuate between easy directions, producing superparamagnetic behavior. Superparamagnetism is desirable for reducing remanent aggregation in injectable formulations but can weaken low-frequency magnetostrictive transduction. The optimum core size is therefore application-specific: small enough for colloidal stability and clearance, but large or anisotropic enough to retain an effective piezomagnetic response. Theoretical descriptions of electric polarization in small magnetic particles and multiscale models of ME nanoparticle composites show that surface stress, depolarization, geometry, and elastic boundary conditions become increasingly important as particle dimensions decrease [12,13].

2.2. Material Systems and Architectures

CFO-BTO is the benchmark core–shell MENP system. Cobalt ferrite provides high anisotropy and magnetostriction, while $BaTiO_3$ provides a lead-free ferroelectric phase. Scalable synthesis studies have shown that commercial or synthesized $CoFe_2O_4$ powders of different sizes and cubic or tetragonal $BaTiO_3$ precursors can be processed into ME composites, with performance depending on phase fraction, annealing, and interfacial quality [14]. Connectivity studies in CFO-BTO ceramics demonstrate a general principle that also applies to nanoparticles: the topology of the two phases controls mechanical load transfer and electrical leakage [15]. A continuous ferrite pathway may increase conductivity and suppress the useful voltage, whereas an electrically insulating ferroelectric phase surrounding separated magnetic regions can improve charge retention. Alternative magnetic cores broaden the design space. $La_{0.7}Sr_{0.3}MnO_3$–$BaTiO_3$ core–shell nanoparticles have shown strain-related changes and enhanced magnetization associated with the core–shell interface [16]. FePt–$BaTiO_3$ hybrid particles combine a metallic magnetic phase with a ferroelectric oxide and illustrate the possibility of multifunctional magnetic, optical, and catalytic behavior [17].

Nanoparticle-based CFO-BTO thin-film heterostructures also demonstrate how preformed particles can be assembled into device-compatible layers for voltage control of magnetism [18]. Nanoparticle-based CFO-BTO thin-film heterostructures are classified here as related ME thin-film devices rather than true core–shell MENPs. They are nevertheless useful for demonstrating how preformed particles can be assembled into device-compatible layers and for extracting transferable information on interface formation, clamping, phase fraction, and electrical contact. The biomedical choice of core must balance magnetic performance and toxicological risk. Cobalt ferrite is robust and strongly magnetostrictive, but dissolution or long-term release of cobalt ions is a concern. Magnetite and maghemite have more established biomedical use, although their smaller magnetostriction may require optimized size, shape, or bias fields. Nickel ferrite and manganese-containing ferrites can tailor coercivity and magnetostriction, but each composition introduces its own ion-release and metabolic questions. Metallic cores such as FeCo or FePt can provide high magnetization but require highly reliable passivation against oxidation and ion release. Several earlier studies established the compositional breadth of oxide core–shell systems.

CFO-BTO nanostructures were synthesized and characterized as multiferroic core–shell materials, while subsequent work examined the magnetodielectric response of CFO-BTO, the room-temperature coupling of $CuFe_2O_4$-$BaTiO_3$, and hydrothermally prepared $NiFe_2O_4$-$BaTiO_3$ with a well-matched interface [19–22]. These studies are important because they show that the interface chemistry and phase purity can be as influential as the nominal bulk properties of the selected ferrite and ferroelectric phases. Amorphous alloy nanoparticles provide a less explored alternative to crystalline ferrites. Co-Fe-Si-B ferroflu-

ids and amorphous Co-Zr-B nanopowders demonstrate that metallic-glass-type particles can be prepared at the nanoscale [23,24]. Their soft-magnetic behavior and potentially large low-field piezomagnetic response could reduce the required bias field, although oxidation, passivation, and formation of a uniform ferroelectric shell remain unresolved. Related PZT nanoparticle synthesis and $CoFe_2O_4$-PZT electrospun nanofibers also illustrate the diversity of piezoelectric architectures available for high-coupling systems, but lead-containing phases require stringent encapsulation and leachability assessment [25,26].

$BaTiO_3$ remains the preferred shell for most biomedical MENPs because it is lead-free and chemically familiar, but its nanoscale ferroelectricity is processing-sensitive. The shell must be sufficiently crystalline and tetragonal to produce a meaningful piezoresponse, yet not so thick that the particle becomes too large or the shell becomes mechanically decoupled. Nanopowder studies of ferroic oxides emphasize the importance of phase purity, grain size, calcination temperature, and defect chemistry when preparing precursors for ME composites [27]. Low-temperature nanoparticle-directed solid-state synthesis offers another route to complex oxides and can reduce the thermal budget that otherwise promotes grain growth and interdiffusion [28]. $BiFeO_3$ is attractive because it is a room-temperature multiferroic and can provide a ferroelectric shell with exchange interactions at a ferrite interface. Its disadvantages include leakage currents, bismuth volatility, secondary phases, and sensitivity to oxygen vacancies. BCZT-type lead-free shells, based on calcium-and zirconium-modified $BaTiO_3$, are increasingly attractive because they can combine high electromechanical response with avoidance of lead.

PZT shells remain useful as a performance benchmark, but their biomedical use should be limited to well-encapsulated or nonimplantable devices unless long-term containment and leach testing are demonstrated. Silica-coated magnetoelectric particles occupy a special category. Silica is widely used for colloidal stabilization, fluorescence loading, and silane chemistry, but conventional amorphous silica is not a strong bulk piezoelectric. Reports of magnetoelectric-silica systems should therefore provide explicit evidence for the electrical transduction mechanism rather than assuming that all silica shells behave as conventional piezoelectrics. In practice, a silica layer may be more valuable as a protective and functionalization coating placed outside an already active ME core–shell structure.

PZT–$CoFe_2O_4$ systems demonstrate the high coupling achievable when a strongly piezoelectric phase is intimately mixed with a magnetostrictive ferrite. In situ sol–gel co-synthesis under controlled pH followed by microwave sintering has been used to improve phase formation and microstructural control [29]. Although such ceramic composites are not directly injectable, the chemistry illustrates how precursor hydrolysis, pH, and thermal treatment determine interfacial reactions. Chemical-bonding assembly of multifunctional oxide nanocomposites provides a complementary strategy in which preformed nanoparticles are linked through controlled surface chemistry, potentially enabling interfaces at lower temperatures and with less interdiffusion [30]. For core–shell particles, an ideal interface should be continuous, thin, mechanically stiff enough to transfer strain, chemically stable, and electrically insulating enough to prevent leakage. A very soft organic interlayer improves colloidal stability but may mechanically isolate the phases. A very rigid inorganic interface may transfer strain efficiently but create residual stress or cracks. Surface ligands used during core synthesis must therefore be removed, exchanged, or transformed without causing uncontrolled aggregation.

Piezoelectric polymers offer flexibility, low acoustic impedance, low-temperature processing, and easier integration with tissues. P(VDF-TrFE)-$CoFe_2O_4$ films have demonstrated self-biased ME behavior for flexible AC magnetic sensing [31], while $CoFe_2O_4$-PVDF 0–3 composites have shown large and approximately linear ME voltage coefficients over selected field ranges [32]. P(VDF-TrFE)–$CoFe_2O_4$ films and $CoFe_2O_4$–PVDF 0–3 composites

are classified as related ME composites/devices because the magnetic particles are dispersed in a piezoelectric matrix rather than organized as discrete core–shell MENPs. Their relevance lies in demonstrating particle–matrix coupling, flexibility, and tissue-compatible integration. In contrast, systems in which verified $BiFeO_3$–$CoFe_2O_4$ core–shell particles are embedded in P(VDF-TrFE) are classified as core–shell-derived systems because the discrete inorganic core–shell unit is retained within the polymer host. Particle dispersion is a central variable. Comparative preparation by ultrasound and surfactant-assisted routes showed that very different agglomeration states did not always produce large changes in macroscopic ME response, suggesting that matrix connectivity and effective mechanical coupling can dominate over visually assessed dispersion alone [33]. More recent work with polyethylene glycol (PEG)-modified $CoFe_2O_4$ particles in PVDF demonstrated smaller agglomerates, lower surface roughness, reduced dipolar interaction fields, and an enhanced local piezoresponse [34]. These results show that surface modification can simultaneously influence colloidal behavior, magnetic interactions, polymer crystallization, and electromechanical coupling.

The electroactive β phase of PVDF is essential for piezoelectricity. In situ studies have shown that ferrite nanoparticles and mechanical stretching can promote the α-to-β transformation [35]. Particle size and concentration likewise affect nucleation of the electroactive phase [36]. Alternative architectures include electrosprayed $CoFe_2O_4$-PVDF microspheres [37], electrospun nanofibers [38], and $NiZnFe_2O_4$-induced β-phase nucleation [39]. Modeling and experimental optimization of polymer–magnetostrictive systems emphasize that filler loading, magnetic blocking, particle rotation, matrix modulus, and electrical boundary conditions all determine the output [40]. Hybrid structures containing $BiFeO_3$-$CoFe_2O_4$ particles in P(VDF-TrFE) further illustrate how an inorganic core–shell unit can be embedded in a flexible piezoelectric matrix to preserve ME coupling during bending [41].

Representative magnetoelectric core–shell and core–shell-derived nanostructures with chemically diverse magnetic and piezoelectric/ferroelectric phases are compared in Table 1. The reported values must be interpreted together with the architecture, sample dimensions, and measurement method because local-probe estimates, nanofiber measurements, and pellet-scale voltage coefficients are not directly interchangeable.

Table 1. Representative magnetoelectric core–shell and core–shell-derived nanostructures grouped by measurement scale and method. Reported values are reproduced as stated in the cited studies and should not be interpreted as directly comparable across measurement classes.

Core Phase	Shell Phase	Architecture Class	Architecture/Synthesis	Reported ME Response/Estimate (mV cm^{-1} Oe^{-1})	Measurement/Conditions	Application/Significance	Ref.
A. Local/nanoscale probe-based measurements—local electrical or electromechanical response							
$CoFe_2O_4$	$BaTiO_3$	True core–shell MENP	≈20 nm spherical MENPs; thermal-decomposition core + sol–gel shell	>5000	Local STM nanoprobe; 0–200 Hz; HDC > 1 kOe	Nanomedicine and brain–machine interfaces	Wang et al. (2020) [6]
$NiFe_2O_4$	$BaTiO_3$	True core–shell MENP	≈20 nm spherical MENPs; thermal-decomposition core + sol–gel shell	>2000	Local STM nanoprobe; 0–200 Hz; HDC > 1 kOe	Nanomedicine; frequency-dependent transduction	Wang et al. (2020) [6]
$CoFe_2O_4$	PZT	Core–shell-derived fibrous system	Coaxial core–shell nanofibers; sol–gel + electrospinning	29,500	Local PFM-based lateral ME estimate under magnetic field	Nanoscale sensors and transducers	Xie et al. (2011) [42]
$CoFe_2O_4$	$BiFeO_3$	True core–shell MENP	Hydrothermal CFO core + sol–gel BFO shell	NR	Field-dependent local PFM response; AC-field catalytic validation	Wireless magnetoelectric catalysis	Mushtaq et al. (2019) [43]
Fe_3O_4	BCZT	True core–shell MENP	Sub-20-nm core–shell NPs; coprecipitation + microwave-assisted hydrothermal shell growth	1.19×10^6	Local nanoscale ME estimate combined with piezoresponse measurements	Nanocatalysis, drug delivery, and cancer therapy	Urakova et al. (2025) [44]
$MnFe_2O_4$	BCZT	True core–shell MENP	Epitaxial ≈4 nm shell on MFO cores; hydrothermal synthesis	1.52×10^6	Local PFM coercive-voltage shift under 500 Oe	Intracellular stimulation and osteogenic differentiation	Mendes et al. (2025) [45]
B. Macroscopic/ensemble direct ME-voltage measurements—effective response of powders, pellets, or sintered structures							
$CuFe_2O_4$	$BaTiO_3$	True core–shell particulate system	Core–shell powder; two-step sol–gel route	22.5	Direct lock-in ME voltage measurement at room temperature	Lead-free multifunctional devices	Thankachan et al. (2018) [21]
$La_{0.7}Sr_{0.3}MnO_3$	$BaTiO_3$	True core–shell MENP	Perovskite–perovskite core–shell nanopowder; sol–gel synthesis	54.5	Transverse direct ME response; HDC ≈1 kOe	Sensors and magnetically controlled devices	Nayek et al. (2013) [16]
PZT	$NiFe_2O_4$	True core–shell MENP (inverse)	Inverse core–shell particulate composite; chemical NFO coating + low-temperature sintering	195	Direct ME voltage; 1 kHz, HAC = 1 Oe; peak near HDC = 454 Oe	Broad-bias magnetic sensing	Islam et al. (2008) [46]
$BNT–BT_{0.08}$	$CoFe_2O_4$	True core–shell MENP (inverse)	Inverse core–shell particles (15–40 nm); two-step wet-chemical sol–gel route	≈0.6	Direct longitudinal ME voltage on sintered core–shell ceramics	Lead-free multifunctional devices	Cernea et al. (2020) [47]

2.3. Key Structure–Property Relationships

Core size influences nearly every stage of the ME cascade. As ferrite particles become smaller, surface spin disorder can reduce saturation magnetization, while thermal fluctuations can drive a transition from blocked ferrimagnetic behavior to superparamagnetism. This can improve redispersibility and reduce remanent clustering, but it also lowers the reproducible low-frequency magnetostrictive response. Fe_3O_4-$BaTiO_3$ studies have shown that larger iron oxide cores exhibit higher coercivity, remanent magnetization, and magnetostriction than smaller cores [8]. Size-dependent ME measurements on Fe_3O_4 nanoparticles similarly confirm that nanoscale coupling is not a simple bulk-property extrapolation [48]. The optimum size must be selected for the intended task. A particle used for magnetic guidance may benefit from a high magnetic moment, whereas an intravenously administered formulation may require a smaller hydrodynamic diameter and low remanence. Neural membrane stimulation can benefit from particles that remain localized at the membrane and produce a strong low-field response. A resonant magnetic sensor may instead exploit frequency-dependent dynamics.

Shape anisotropy offers an additional degree of freedom: rods, cubes, flowers, and elongated cores can increase magnetic anisotropy and directional magnetostriction, but they may also alter cellular uptake and clearance.

A thin shell minimizes particle size and can produce a high electric field for a given charge density, but discontinuous coverage increases leakage and exposes the magnetic core. A thick shell improves chemical isolation and drug-loading area but reduces the magnetic mass fraction and can become polycrystalline. HRTEM studies show that the maximum thickness of a single-crystalline $BaTiO_3$ coating depends on core morphology and may be limited to a few tens of nanometers [49]. In $ZnFe_2O_4$–$BaTiO_3$ particles, an unfavorable core-to-shell thickness ratio and nonuniform strain were associated with electrical instability [50]. The ratio also changes the mechanical neutral axis and stress distribution. In a spherical inclusion, the core may be strongly constrained by a stiff shell, reducing free magnetostriction but increasing transferred stress. If the shell is too compliant or cracked, the core deforms without generating useful polarization.

Aggregation is often treated only as a colloidal problem, but it also changes transduction. Closely spaced magnetic cores interact through dipolar fields, modifying coercivity and magnetostriction. Mechanical contacts between particles can create collective strain pathways, while electrical contacts can create leakage. An agglomerate may therefore exhibit a stronger or weaker apparent ME signal than isolated particles. Recent local KPFM measurements on CFO-BTO analyzed agglomerated regions and emphasized that the measured surface-potential modulation represented local composite behavior rather than a single isolated shell [9]. In polymer matrices, aggregation can locally increase filler fraction and stress concentration. PEG modification has been shown to reduce agglomerate size and dipolar interaction while increasing local piezoresponse [34]. Yet perfect dispersion is not always the sole objective: a controlled percolative mechanical network may enhance strain transfer before electrical leakage becomes dominant. The optimum microstructure may therefore involve small, well-separated clusters rather than completely isolated particles.

ME response depends on frequency because magnetic relaxation, domain-wall motion, dielectric loss, ionic screening, and the measurement circuit all change with the time scale. Low-frequency operation is attractive for neural and cellular stimulation because it reduces inductive and heating losses, but ionic screening can attenuate static surface fields. Higher frequencies can increase dynamic charge but may produce magnetic heating and tissue exposure concerns. A DC bias can position the core at the maximum piezomagnetic slope; however, bias magnets increase device size and can promote aggregation. Mechanical boundary conditions are equally important. A particle adhered to a rigid substrate, embed-

ded in a hydrogel, internalized in an endosome, or attached to a soft cell membrane will experience different clamping. This can change both the core strain and the shell voltage. Biological experiments should therefore identify particle localization and, where possible, model the local mechanical environment. The same MENP dose can produce different effects depending on whether particles remain extracellular, bind to the plasma membrane, or are internalized.

A predictive structure–property model should couple magnetic hysteresis, magnetostriction, elasticity, piezoelectricity, dielectric screening, particle orientation, and biological geometry. Multiscale analytical models provide a foundation [13], but experimental validation is still limited. Machine-learning approaches could eventually connect synthesis variables and microscopy descriptors to ME output, provided that datasets use standardized definitions and include negative results. Until then, systematic factorial studies of core size, shell thickness, interface chemistry, and field conditions are more valuable than isolated reports of a single optimized sample.

3. Synthesis, Processing, and Surface Engineering

3.1. Core Synthesis and Oxide-Shell Formation

Core synthesis should be treated as the first stage of ME device engineering rather than as an isolated nanoparticle problem. The selected method determines particle size distribution, crystallinity, cation occupancy, surface ligands, magnetic anisotropy, and subsequent shell nucleation. Co-precipitation is inexpensive and readily scalable, but rapid nucleation and variable local pH can yield polydisperse ferrites with hydroxyl-rich surfaces. These surfaces can be advantageous for oxide shell growth, although poorly controlled washing may leave ionic residues that alter dielectric behavior. Thermal decomposition offers monodisperse and highly crystalline particles, but the hydrophobic oleate-or amine-terminated surface must be transferred to a polar medium before growth of $BaTiO_3$, $BiFeO_3$, or another oxide shell. Hydrothermal and solvothermal synthesis can produce faceted, rod-like, or flower-like cores and can be coupled directly to shell deposition, but the resulting products often require careful separation of isolated particles from fused aggregates. For biomedical use, the synthesis target should include a hydrodynamic specification in addition to the TEM core size. Polyol synthesis provides an additional route for tuning $CoFe_2O_4$ particle size, crystallinity, and magnetic properties while retaining dispersibility [51].

A nominally 20 nm ferrite particle may form 100–500 nm clusters after ligand exchange or shell growth. The magnetic core should therefore be characterized before and after every chemical transformation. Saturation magnetization normalized to the magnetic-phase mass, coercivity, remanence, blocking temperature, and AC susceptibility are particularly informative. A decline in magnetization after coating is expected because of the nonmagnetic shell, but an unexpectedly large decline may indicate oxidation, cation redistribution, or formation of secondary phases.

Sol–gel processing is among the most common strategies for forming $BaTiO_3$ around ferrite seeds. A titanium alkoxide is hydrolyzed and condensed in the presence of a barium precursor and dispersed magnetic cores. The reaction rate must be slow enough to favor heterogeneous nucleation on the core rather than homogeneous precipitation of free $BaTiO_3$. Water content, pH, solvent polarity, chelating agents, precursor addition rate, and core-surface chemistry determine whether the product is a uniform shell, an island coating, or a mixture of separate phases. Subsequent calcination crystallizes the perovskite phase but can cause sintering, core oxidation, interdiffusion, or formation of $BaFe_{12}O_{19}$ and other parasitic phases. A useful strategy is to employ a thin amorphous precursor layer followed by controlled crystallization. This can improve coverage, but the shrinkage associated with drying and crystallization may generate cracks. Repeated deposition cycles allow

shell-thickness control, although each cycle increases the probability of aggregation. The shell-growth chemistry should therefore be evaluated using both population-level methods and single-particle microscopy. Reporting only the coexistence of ferrite and perovskite peaks in XRD is insufficient to prove a core–shell structure.

As a representative sol–gel coating approach, Dhanyaprabha et al. [52] prepared $NiFe_2O_4$–$BaTiO_3$ core–shell composites by dispersing preformed $NiFe_2O_4$ cores in a $BaTiO_3$ precursor sol, followed by drying and calcination to crystallize the ferroelectric phase around the ferrite particles. A representative sol–gel synthesis route for $NiFe_2O_4$–$BaTiO_3$ core–shell nanoparticles is schematically illustrated in Figure 2. The magnetic-core fraction was systematically varied to examine its influence on the resulting structure and properties. Importantly, however, the coexistence of ferrite and $BaTiO_3$ phases does not by itself confirm a true core–shell morphology; direct TEM/STEM elemental mapping is required to verify continuous shell formation.

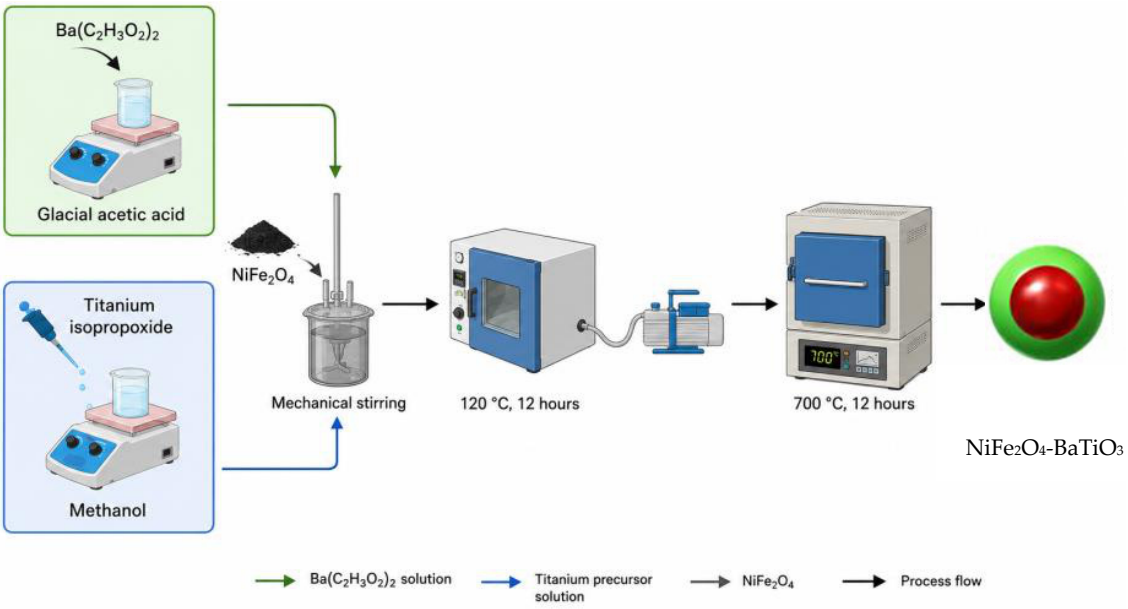


Figure 2. Representative sol–gel synthesis route for $NiFe_2O_4$-$BaTiO_3$ core–shell nanoparticles, based on the procedure described in Ref. [52]. The process includes precursor preparation, mixing with $NiFe_2O_4$ cores, vacuum drying at 120 °C for 12 h, and calcination at 700 °C for 12 h.

Hydrothermal growth provides direct access to crystalline $BaTiO_3$ at lower temperatures than conventional solid-state reactions. Ferrite seeds are dispersed with barium and titanium precursors in a strongly alkaline solution, and temperature, time, mineralizer concentration, and seed morphology control nucleation. Hydrothermal processing has been used to produce $BaTiO_3$ coatings whose crystallinity changes from single-crystalline to polycrystalline as the shell thickens [49]. The method can preserve discrete particles when the seed concentration and reaction kinetics are well controlled, but it can also generate large secondary $BaTiO_3$ crystals and strongly fused agglomerates. Solvothermal methods are similarly useful for Fe_3O_4-$BaTiO_3$ and other core–shell-like structures. Organic solvents can slow hydrolysis and improve particle dispersion. However, residual organics, surfactants, and high-boiling solvents must be removed before biological testing. The cleaning process should be validated by thermogravimetric analysis, infrared spectroscopy, elemental analysis, and endotoxin testing where appropriate.

3.2. Assembly, Polymer Processing, and Hierarchical Encapsulation

Not every functional architecture requires direct epitaxial shell growth. Preformed magnetic and piezoelectric nanoparticles can be assembled through electrostatic attraction, silane coupling, polymer bridging, or chemical bonding. Such assembly can reduce the thermal budget and permit independent optimization of each phase. The cost is a more complex mechanical interface and a greater risk that an organic coupling layer will attenuate strain. Chemical-bonding approaches are particularly attractive when they create short, dense linkers rather than thick polymer cushions [30]. A second strategy is hierarchical encapsulation. An active inorganic core–shell particle can be coated with silica, PEG, phospholipids, proteins, or cell membranes. The inner interface is then optimized for ME coupling, while the outer interface is optimized for biological stability and targeting. This separation of functions is conceptually preferable to asking a single shell to provide strong piezoelectricity, colloidal stability, molecular recognition, and immune evasion simultaneously. The outer coating should be thin enough to preserve the local electrical interaction and should not prevent the particle from approaching the target membrane or biomolecule.

For polymer-based ME systems, solvent casting, electrospinning, electrospraying, compression molding, and additive manufacturing offer complementary architectures. Solvent casting is simple and allows systematic control of filler fraction, but solvent evaporation can drive phase separation and sedimentation. Electrospinning produces high-surface-area fibrous scaffolds and can orient polymer chains, promoting the electroactive phase. Electrospraying generates microspheres that can serve as carriers or injectable building blocks. Mechanical stretching and compression can increase PVDF β-phase content and improve particle–matrix contact. In hydrogels, particles can be mixed before cross-linking, conjugated to the network, or loaded into porous regions after gel formation. For tissue engineering, the preparation method must preserve both transduction and biological transport. A highly loaded, dense composite may produce a strong electrical output but restrict nutrient diffusion, cell infiltration, or biodegradation. Conversely, a porous hydrogel may be biologically favorable but mechanically too soft to transfer magnetostrictive strain. The optimum structure is therefore often a multiscale composite: active nanoparticles create local electrical cues, while the macroscopic scaffold provides tissue-level mechanics and mass transport. The main preparation strategies for MENPs and related architectures are summarized in Table 2, together with their key processing variables, advantages, and limitations. The appropriate method should therefore be selected according to the required particle architecture, crystallinity, scalability, and intended biomedical application.

Table 2. Preparation strategies and their principal control variables.

Method	Typical Role	Critical Variables	Advantages	Limitations
Co-precipitation	Ferrite-core synthesis	pH, ionic strength, addition rate, oxidation state	Low cost; aqueous; scalable	Polydispersity; defects; residual ions
Thermal decomposition	Monodisperse magnetic cores	Ligand chemistry, heating rate, precursor ratio	High crystallinity; narrow size distribution	Hydrophobic surface; ligand-exchange requirement
Sol–gel coating	$BaTiO_3$, PZT, or $BiFeO_3$ shell formation	Hydrolysis rate, chelation, pH, calcination	Composition control; compatible with multiple cores	Free secondary particles; cracking; thermal interdiffusion

Table 2. *Cont.*

Method	Typical Role	Critical Variables	Advantages	Limitations
Hydrothermal/ solvothermal growth	Crystalline oxide shells or nanorods	Temperature, alkalinity, solvent, seed density	Good crystallinity; shape control	Pressure equipment; batch sensitivity; agglomeration
Chemical assembly	Coupling preformed phases	Surface charge, linker length, grafting density	Low temperature; modular design	Organic layer may reduce strain transfer
Electrospinning/ electrospraying	Fibers and microspheres	Viscosity, field, flow rate, particle dispersion	Flexible, porous, high-area constructs	Not strict core–shell; loading and alignment limits
Hydrogel encapsulation	3D tissue-engineering constructs	Cross-link density, particle loading, pore structure	Soft, hydrated, cell-compatible	Mechanical damping; diffusion and sterilization challenges

3.3. Surface Coatings, Biomolecular Conjugation, and Targeting

The outer surface determines whether an ME particle remains dispersed, reaches the intended tissue, binds to a target, is internalized, or is removed by the immune system. It also determines the electrical distance between the active piezoelectric phase and the biological membrane. Surface engineering must therefore be treated as part of the transducer rather than as a cosmetic post-processing step. In a lead-free CFO–BCZT system evaluated for nervous-tissue stimulation, the core–shell composition was selected not only for ME activity but also for improved biocompatibility relative to lead-containing alternatives [53]. This illustrates the need to optimize material composition and biological interface together. A practical architecture may contain three concentric functions: a magnetostrictive core, an electromechanically active shell, and a thin biological interface layer. The third layer can provide steric stabilization, reactive groups, fluorescence, targeting, or immune camouflage. It should be continuous enough to prevent dissolution yet thin and compliant enough to preserve strain and local electric-field coupling.

Silica is widely used because silanol groups support silane chemistry, fluorophores can be incorporated, and the surface can be modified with amines, thiols, or carboxyl groups. Magnetoelectric-silica nanoparticles have been developed as fluorescent and T2-weighted MRI-visible carriers for on-demand doxorubicin delivery [54]. The system illustrates the value of combining magnetic contrast, optical tracking, and drug release in one platform. For a general MENP design, silica is especially useful as an outer protective coating over an active oxide shell. Its thickness should be minimized and its porosity controlled because a thick insulating layer can attenuate electrical interactions and delay drug release. PEG provides steric stabilization and can reduce nonspecific protein adsorption and aggregation. In ferrite/PVDF composites, PEG modification improved particle distribution and local electromechanical response [34]. In injectable systems, PEG chain length and grafting density influence circulation time, protein corona, cell uptake, and access of targeting ligands. Excessive PEGylation can create a “stealth” particle that also binds poorly to target cells, so cleavable or mixed-density coatings may be advantageous.

The broader nanoparticle drug-delivery literature provides a mature toolbox for engineering this outer layer. Polymeric carriers, iron-oxide particles, and multifunctional magnetic nanoparticles have been functionalized with poly(L-lysine), poly(lactic-co-glycolic acid), amphiphilic polymers, surfactants, and carbodiimide-based coupling chemistries to control circulation, cellular uptake, and sustained or targeted drug release [55–61]. These studies are not intrinsically magnetoelectric, but their lessons on ligand density, colloidal

stability, loading efficiency, and release kinetics are directly transferable to MENP design. For an ME particle, however, the outer coating must satisfy an additional requirement: it should not mechanically decouple the active shell from its environment or screen the electrical signal so strongly that the biological interface receives no useful stimulus. Surface chemistry should therefore be optimized jointly with the ME response. Reporting only drug loading or zeta potential before and after coating is insufficient; the magnetic, piezoelectric, and field-induced electrical responses should also be measured after every functionalization step.

For biosensing, the surface must carry a recognition element such as an antibody, aptamer, peptide, carbohydrate, nucleic-acid probe, or molecularly imprinted polymer. The ideal coupling chemistry preserves the orientation and affinity of the receptor while maintaining access to the active shell. Amine–carboxyl coupling is convenient but can randomly orient antibodies. Protein A/G, click chemistry, biotin–streptavidin, and site-specific peptide tags provide better orientation control. The receptor density must be high enough for capture but low enough to avoid steric blocking and to preserve colloidal stability. Physical models of targeted anticancer delivery by MENPs have proposed that electric-field interactions, membrane capacitance, and conductivity differences can contribute to selective particle–cell attraction [62]. More recent theoretical work has examined tumor-specific targeting in terms of conductivity and capacitance contrasts [63]. These mechanisms are intriguing but should not be treated as substitutes for validated receptor chemistry. In heterogeneous biological fluids, nonspecific electrostatic effects compete with proteins, salts, and extracellular matrix components.

A clinically credible platform should combine physical targeting with molecular recognition and should quantify specificity against closely related off-target cells.

Hydrogel encapsulation can localize MENPs, prevent systemic dispersion, and create a tissue-like mechanical environment. BBB-penetrating MENP formulations combined with a sustained gel have been investigated for postoperative glioma therapy, illustrating how a local depot can integrate magnetic targeting, drug delivery, and prolonged exposure [64]. Extracellular-vesicle-based magnetoelectric therapeutics have also been proposed for latency targeting in HIV treatment [65]. These systems shift the design problem from an isolated nanoparticle to a hierarchical therapeutic carrier. Cell-membrane camouflage provides another route to selective interaction. Dendritic-cell-membrane-coated CFO-$BiFeO_3$ particles were engineered to target CD4+ T cells and, under magnetic stimulation, promoted a TAF9B-dependent T-helper-2 program that reduced inflammation in animal models [66]. A Parkinson's disease platform used a biomimetic membrane around CFO-BTO material to enhance blood–brain barrier penetration, drug delivery, and electrical stimulation [67]. These studies show that biomimetic surfaces can add biological addressability, but they also introduce variability in membrane composition, storage stability, pathogen safety, and manufacturing.

4. Characterization and Magnetoelectric Measurement

4.1. Structural, Chemical, and Colloidal Characterization

A convincing core–shell assignment requires complementary methods. X-ray diffraction identifies crystalline phases and can quantify lattice parameters, crystallite size, and phase fraction through Rietveld refinement. It cannot by itself determine whether one phase surrounds another. Broad peaks from nanoscale materials and overlapping ferrite/perovskite reflections can conceal minor secondary phases. Raman spectroscopy is valuable for distinguishing tetragonal and cubic $BaTiO_3$, identifying $BiFeO_3$-related modes, and detecting carbonaceous or organic residues. Fourier-transform infrared spectroscopy can verify polymer phases and surface ligands, but its interpretation should be supported

by thermal or chemical analysis. Transmission electron microscopy remains the principal method for visualizing shell coverage and thickness. High-angle annular dark-field scanning TEM and elemental mapping are especially important because conventional bright-field contrast can misidentify overlapping particles as a shell. A robust analysis should include a statistically meaningful number of particles, shell-thickness distributions, and images from multiple batch regions. Electron diffraction or lattice-resolved TEM can verify that both core and shell are crystalline.

Electron tomography, although less commonly used, is valuable for distinguishing a true three-dimensional shell from a two-dimensional projection of an aggregate. Scanning electron microscopy provides population-level morphology and is particularly useful for polymer films, fibers, hydrogels, and dried agglomerates. Atomic force microscopy provides surface roughness, particle height, and mechanical contrast, while magnetic force microscopy can identify magnetic domains or core locations. In scanning probe studies of CFO–BTO particles, phase and magnetic-force images revealed an intermediate region between core and shell that would be difficult to resolve by conventional diffraction alone [68]. Such transition regions may be beneficial if they provide graded elastic matching, or detrimental if they are chemically disordered and electrically leaky.

Energy-dispersive X-ray spectroscopy, electron energy-loss spectroscopy, and X-ray photoelectron spectroscopy can confirm elemental distribution and oxidation states. XPS is particularly useful for detecting Fe^{2+}/Fe^{3+}, Co^{2+}/Co^{3+}, oxygen vacancies, surface hydroxylation, and the success of silane or polymer coatings. Because XPS probes only a shallow surface depth, a strong magnetic-core signal from a nominally thick shell may indicate incomplete coverage. Inductively coupled plasma mass spectrometry should be used to quantify total composition, metal-ion release, and batch-to-batch stoichiometry. Dynamic light scattering provides hydrodynamic diameter and polydispersity in suspension, whereas TEM reports the dry inorganic dimensions. Both values are needed. Zeta potential offers a first measure of colloidal stability and surface charge, but it depends strongly on pH, ionic strength, and the measurement model. Stability should be tested in water, buffer, serum-containing medium, and the intended administration formulation over relevant time periods. Nanoparticle tracking analysis, analytical ultracentrifugation, and field-flow fractionation can help resolve multimodal populations that are hidden by intensity-weighted DLS.

Zeta-potential values are highly dependent on the composition of the liquid phase, pH, ionic strength, and the position of the slipping plane. Consequently, a single value measured in deionized water cannot be treated as an intrinsic material constant or used to predict stability in serum. The solvent and dispersant, equilibration time, temperature, conductivity, pH, concentration, and measurement model should be reported, and measurements should be repeated in the formulation and biological medium relevant to the intended application [69]. Surface area and porosity matter for drug loading and biomolecular conjugation. Brunauer–Emmett–Teller analysis is useful for dried powders, but accessible surface area in a hydrated protein-containing environment may be very different. Thermogravimetric analysis can quantify organic coatings, while fluorescence or radiolabeling can track ligand density. A complete functionalization report should state the coupling chemistry, ligand-to-particle ratio, unbound-ligand removal method, and number of recognition molecules per particle.

4.2. Magnetic, Electromechanical, and Macroscopic ME Measurements

Vibrating-sample magnetometry or SQUID magnetometry should report magnetization versus field at the biological operating temperature and, when relevant, temperature-dependent zero-field-cooled and field-cooled curves. Mass normalization must specify

whether it refers to the entire core–shell particle or only the magnetic phase. Coercivity and remanence affect both transduction and aggregation. AC susceptibility can reveal magnetic relaxation and heating regimes. Magnetostriction is difficult to measure directly for isolated nanoparticles; indirect composite-based approaches can estimate it, but uncertainty in matrix transfer should be included [70]. Ferroelectric characterization of nanoscale shells is more difficult than that of bulk ceramics. Polarization–electric-field loops measured on pellets can be dominated by leakage, interparticle capacitance, and electrode effects. Piezoresponse force microscopy provides local amplitude and phase, switching spectroscopy, and domain imaging. However, electrostatic forces, ionic motion, surface charging, and tip–sample contact mechanics can mimic piezoresponse. A reliable study should include nonpiezoelectric controls, frequency dependence, on-field and off-field measurements, and repeated cycling.

PFM is strongest when used comparatively—for example, to determine whether magnetic-field application changes local electromechanical response—rather than as the sole basis for a quantitative bulk coefficient.

The conventional direct ME measurement applies a small AC magnetic field, often superimposed on a DC bias, and records the induced voltage with a lock-in amplifier. For a dense laminate, α_E can be calculated from sample thickness and field amplitude. For nanoparticle powders, the situation is more complicated. Pellets contain voids, random particle orientations, interparticle contacts, leakage paths, and an effective dielectric medium. Pressing pressure and binder content alter the result. If the particles are dispersed in a polymer, the measured coefficient represents the composite, not the isolated particle.

A representative pellet-based measurement workflow is shown in Figure 3. MENP powders may be compacted using a 10-ton uniaxial press into pellets approximately 13 mm in diameter and 0.9 mm thick. The opposing flat faces are metallized (for example, with Au) or coated with conductive silver paint, and electrical leads are attached using conductive silver contacts before connection to a lock-in amplifier. A sinusoidal AC magnetic field, H_{AC}, is generated by Helmholtz coils and calibrated with a gaussmeter, while an electromagnet supplies the variable DC bias field. At a fixed frequency and bias, the induced voltage V is recorded as a function of H_{AC}. The apparent ME voltage coefficient is obtained from $\alpha_E = V/(H_{AC}\, t)$, or equivalently from the slope of the V- H_{AC} curve divided by the pellet thickness t. The measurement is repeated over frequency and DC-bias sweeps to identify the operating point and any resonant enhancement. Computer-controlled acquisition improves repeatability, and thermocouples should continuously monitor the electromagnet, Helmholtz coils, and ambient region to exclude thermal drift.

Sample orientation must also be reported; for a perpendicular configuration, the AC and DC fields are normal to the pellet plane. The lock-in reference harmonic should be stated explicitly. Because a compacted pellet represents an ensemble of particles with finite porosity and interparticle contacts, the measured coefficient is an effective composite value rather than an intrinsic single-particle coefficient.

Inductive pickup is a major concern because the sample electrodes and leads form a loop in a time-varying magnetic field. Measurements should reverse the sample orientation, use twisted and shielded leads, minimize loop area, and include a dummy capacitor or a non-ME control with similar impedance. The measured voltage should scale appropriately with sample dimensions and phase fraction. A true strain-mediated signal should show a physically plausible dependence on magnetic bias and should correlate with the derivative of magnetostriction. Temperature should be monitored to exclude magnetothermal or magnetopyroelectric contributions. The distinction between open-circuit voltage, electric field, charge, and surface potential must be maintained. A lock-in voltage across a pellet can be converted to an apparent α_E only if the active thickness and field distribution are

defined. A surface-potential change measured by Kelvin probe force microscopy is a local electrical signature, not automatically a full ME voltage coefficient.

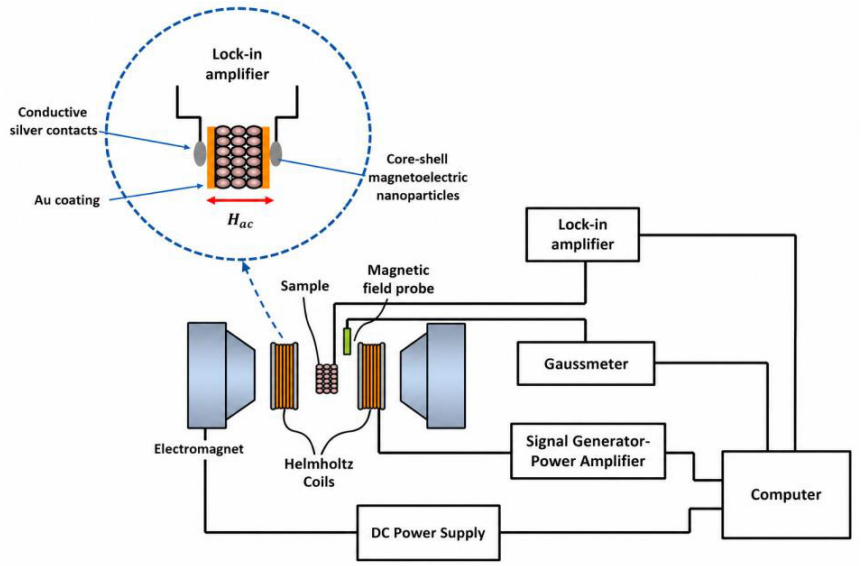


Figure 3. Schematic of a macroscopic magnetoelectric measurement system for a compacted core–shell nanoparticle pellet. Helmholtz coils generate the AC magnetic field, an electromagnet provides the DC bias, a gaussmeter monitors the field, and the induced voltage is measured with a lock-in amplifier. Author-created schematic based on the ME measurement setup used in our laboratory.

Recent CFO-BTO work explicitly treated KPFM as a complementary proof-of-concept method and reported local surface-potential modulation under AC magnetic excitation rather than claiming a universal coefficient [9]. This cautious terminology should become standard.

4.3. Single-Particle, Local-Probe, and Complementary Readouts

Single-particle-level and local-probe measurements have been developed to minimize two important limitations of conventional pellet-based measurements: electrical leakage through the magnetic phase and ensemble averaging over particles with different sizes, orientations, interfaces, and electrical environments. A representative approach was reported by Wang et al. [6], who deposited a thin layer of core–shell magnetoelectric nanoparticles on a highly oriented pyrolytic graphite (HOPG) substrate and established a nanoscale electrical contact using a Pt/Ir scanning tunneling microscopy (STM) probe. A permanent magnet integrated into the scanner supplied a DC bias field above 1000 Oe, while a multi-turn coil surrounding the probe–sample contact generated a perpendicular AC magnetic field of up to approximately 100 Oe. In addition to STM-based local-voltage measurements, magnetic-field-assisted PFM can be used to evaluate field-induced changes in the local electromechanical response, as schematically illustrated in Figure 4.

Using the STM-based nanoprobe configuration reported by Wang et al. [6], approximately 20 nm CFO-BTO and $NiFe_2O_4$–$BaTiO_3$ core–shell nanoparticles were investigated. Maximum ME coefficients above 5 V cm^{-1} Oe^{-1} and 2 V cm^{-1} Oe^{-1} were reported for the Co-ferrite-and Ni-ferrite-based particles, respectively [6]. These unusually high values were attributed to efficient strain transfer across a structurally coherent or lattice-matched core–shell interface, together with the suppression of macroscopic charge-leakage pathways in the local-probe geometry. The two compositions exhibited markedly different frequency dependences. CFO-BTO particles showed an ME coefficient of approximately 6 V cm^{-1} Oe^{-1} in the near-DC regime, followed by a gradual decrease, particularly above approximately

100 Hz. In contrast, the near-DC response of $NiFe_2O_4$–$BaTiO_3$ was below 0.1 V cm^{-1} Oe^{-1} but increased strongly with frequency, exceeding 2 V cm^{-1} Oe^{-1} at 200 Hz.

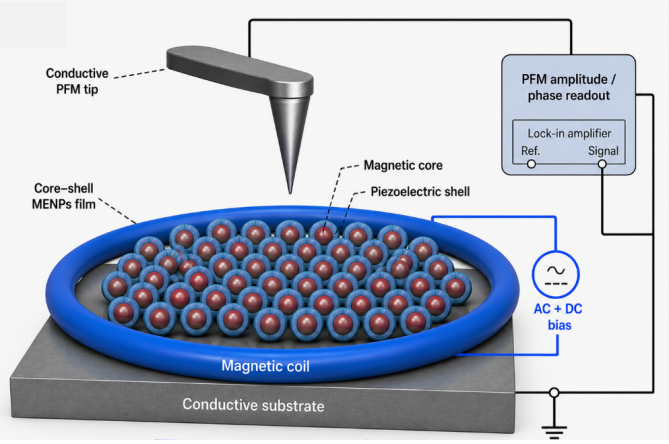


Figure 4. Author-created schematic illustration of magnetic-field-assisted piezoresponse force microscopy for local characterization of core–shell magnetoelectric nanoparticles. A conductive PFM probe measures the local amplitude and phase response in the absence and presence of an external magnetic field.

Magnetic-field-assisted piezoresponse force microscopy can provide complementary information by comparing the electromechanical amplitude and phase before and during magnetic excitation. Kelvin probe force microscopy and electrostatic force microscopy can similarly map local surface-potential and charge variations. However, these techniques remain sensitive to humidity, work-function differences, trapped charge, electrostatic forces, and tip contamination. Correlative measurements in which the same particle is examined by high-resolution TEM, magnetic force microscopy, PFM, and KPFM would therefore be especially valuable for directly linking core position, shell thickness, interfacial crystallinity, magnetic state, and local electrical response.

Reviews of magnetoelectric coefficient measurements emphasize that leakage, capacitive coupling, and circuit artifacts can mimic genuine coupling; artifact controls are therefore essential when interpreting local or macroscopic signals [71].

Optical characterization can provide indirect information on particle composition, absorption, and potential photothermal cross-talk. Cobalt ferrite and CFO–BTO particles have been investigated in the infrared to determine how the shell alters absorption and scattering [72,73]. Optical methods may also contribute to biosensing. A magnetoelectric nanoparticle can support coupled electric and magnetic multipoles, and theoretical or experimental work on chiroptical scattering indicates that such coupling can amplify otherwise weak optical signatures [74]. These approaches are still largely outside mainstream biomedical MENP sensing, but they suggest routes to hybrid magnetic–electrical–optical readout. Thermal effects must also be separated from direct ME coupling. Magnetic nanoparticle–ferroelectric polymer composites can exhibit a magnetopyroelectric response in which magnetic heating changes polarization through the pyroelectric effect [75]. In a biological experiment, both pathways may coexist: an AC magnetic field can produce magnetostriction and heat, while temperature changes can affect membrane potential and cell metabolism. Temperature-matched controls and frequency regimes below significant magnetic loss are therefore essential when the claimed mechanism is purely magnetoelectric. The principal characterization and ME measurement methods discussed above are summarized in Table 3, together with the information they provide, their main strengths, and potential limitations. Complementary techniques are generally required to reliably verify both the core–shell structure and the ME response.

Table 3. Characterization and magnetoelectric measurement methods.

Method	Information Obtained	Key Strengths	Principal Artifacts or Limitations	Refs.
XRD/Rietveld	Phase identity, lattice parameters, crystallite size, phase fraction	Population-level and quantitative	Does not prove core–shell geometry; peak overlap	[47,52]
TEM/STEM-EDS/EELS	Core–shell morphology, thickness, interface, elemental distribution	Direct nanoscale imaging	Projection artifacts; limited sampled population; beam damage	[1,49,52]
DLS/zeta potential	Hydrodynamic size, polydispersity, surface charge	Relevant to biological suspension	Model-dependent; intensity bias toward aggregates	[69]
VSM/SQUID/AC susceptibility	Magnetization, coercivity, blocking, relaxation	Defines magnetic operating regime	Mass-normalization and aggregation effects	[8,51,72]
PFM/switching spectroscopy	Local electromechanical response and domains	Nanoscale spatial resolution	Electrostatic, ionic, and contact-mechanical artifacts	[42,43,50]
KPFM/electrostatic force microscopy	Surface-potential or charge changes	Local electrical readout under magnetic field	Not a direct universal α_E; work-function and humidity sensitivity	[9,68]
Lock-in ME voltage measurement	Composite voltage coefficient versus bias and frequency	Sensitive and widely used	Inductive pickup, leakage, geometry and pellet effects	[16,21,46,71]
Optical/IR spectroscopy	Absorption, scattering, coupled optical modes	Noncontact and potentially multiplexed	Usually indirect evidence of ME coupling	[72–74]

5. Biosensing Principles

A biosensor requires more than a biological effect. It must contain a recognition or interaction element, a transduction mechanism, and a measurable output that can be calibrated against an analyte or biological state. MENPs can participate in several biosensor configurations: as freely dispersed transducers, as labels captured on a surface, as embedded elements in a flexible or microfluidic device, or as local reporters of bioelectric activity. The strongest evidence to date concerns magnetic-particle localization and neural-field sensing rather than direct molecular assays for proteins or nucleic acids. A recent physics-based analysis of MENP-enabled brain–computer interfaces described direct ME conversion for neuromodulation and converse ME conversion for recording [76]. In the recording concept, electric fields associated with neuronal activity perturb the magnetic state of membrane-associated particles, and the resulting magnetic change is detected externally. The approach offers an appealing route to wireless bidirectional interfaces, but neural recording remains less experimentally mature than stimulation. The weak biological signal, particle-orientation distribution, tissue attenuation, and magnetic background all impose demanding signal-to-noise requirements.

Computational studies have examined how MENP concentration and spatial distribution affect peripheral-nerve activation [77] and how ensembles of particles could support minimally invasive brain stimulation [78]. Although these are actuation studies, the same models help define sensing sensitivity because the direct and converse modes share material parameters. Resonant core–shell MENPs have also been proposed as sensors of neural magnetic activity [79]. Such concepts could complement electroencephalography, magnetoencephalography, and intracortical electrodes by bringing the transducer close to the source. The core challenge is that neural magnetic fields are extremely weak and occur in a noisy environment. A particle-based sensor must convert a local biological field into a magnetic or electrical change that can be separated from the external excitation used to interrogate the particle. Resonant detection, modulation at a known carrier frequency, differential measurement, and lock-in amplification are likely to be necessary. The sensing

model should include thermal magnetic noise, Brownian motion, magnetic relaxation, field inhomogeneity, and the stochastic number of particles near each neuron.

MENPs can also function as magnetic labels detected by a separate ME sensor. Thin-film ME devices based on the delta-E effect have been used to map magnetic nanoparticles and magnetically labeled cells [80]. In this configuration, the nanoparticle does not need to generate a large local electric field; it serves as a magnetic marker, while the integrated ME resonator performs the readout. Distance-dependent magnetic nanoparticle detection has been demonstrated with ME sensors for clinical-intervention concepts [81]. Numerical and experimental mapping of colored magnetic particles provides a framework for reconstructing spatial distributions from sensor data [82]. Adaptive mapping models can improve localization when the sensor response and particle position are nonlinear [83]. These approaches are relevant to biosensing because magnetic labels can be conjugated to antibodies, nucleic-acid probes, or cells. The ME sensor then detects label accumulation without optical access. The principal advantages are low optical background, compatibility with opaque samples, and potential integration with microfluidics. The limitations are magnetic background, label nonspecificity, calibration with distance, and the need for robust inverse models.

Magnetic manipulation can be combined with secondary readouts to quantify captured material. Infrared-driven rapid quantification of magnetophoretically trapped drug illustrates how magnetic particles can concentrate an analyte or carrier in a defined region before detection [84]. A MENP-based biosensor could similarly combine magnetic enrichment with an electrical, optical, or resonant readout. This is particularly attractive for low-abundance targets because the particles provide both preconcentration and transduction.

The material platform is theoretically suitable for molecular detection. Binding of a target to a functionalized shell can change particle mass, interfacial stiffness, dielectric environment, surface charge, hydrodynamic drag, or interparticle spacing. Each of these changes can modulate the ME response. In a resonance-based sensor, target binding could shift frequency or quality factor. In a local surface-potential sensor, binding could change ionic screening and the magnetically induced potential. In an aggregation assay, analyte-induced clustering could alter magnetic interactions and the ensemble ME coefficient. Despite this wide design space, direct demonstrations of isolated core–shell MENPs detecting specific proteins, nucleic acids, pathogens, or clinical cancer biomarkers remain sparse compared with drug-delivery and stimulation studies. Many publications use the term "biosensing" broadly to include biological stimulation, magnetic labeling, or cell monitoring. This gap should be stated explicitly because it defines a major opportunity for the field. Future molecular-sensing studies should report calibration curves, limit of detection, linear range, selectivity against interferents, matrix recovery, assay time, storage stability, and comparison with established methods.

For protein detection, antibodies or aptamers can be attached to a thin outer coating. Target binding could be converted into a change in local capacitance or mechanical load. For nucleic acids, complementary probes can create sequence-dependent hybridization, while catalytic amplification or CRISPR-assisted cleavage could change particle clustering. Pathogen assays can use multivalent recognition to promote aggregation or capture onto an ME resonator. Cancer biomarkers can be targeted using aptamers or peptides, but nonspecific adsorption in serum must be controlled with antifouling layers and reference particles.

Because direct quantitative molecular biosensing using isolated core–shell MENPs remains sparse, Table 4 separates experimentally demonstrated ME-sensor-assisted magnetic-labeling and preconcentration approaches from theoretical or computational MENP sensing concepts. Where available, target/analyte, recognition or labeling strategy, sample matrix, detection threshold, and discrimination/selectivity are reported.

Table 4. Quantitative and maturity-based comparison of biosensing-related configurations discussed in this review. Experimental ME-sensor-assisted approaches are separated from theoretical/computational MENP sensing schemes. NR indicates not reported in the cited study.

Configuration/Target or Analyte	Recognition Ligand/Labeling Strategy	MENP or ME Platform	Sample Matrix	Detection Principle	LOD/Detection Threshold	Selectivity/Discrimination	Ref.
A. Experimental or experimentally grounded biosensing-related approaches							
Magnetic label mapping: SPION distribution and SPION-labeled fibroblast cells	Cell-associated magnetic labeling; no molecular recognition ligand used	Related ME device: thin-film ΔE-effect ME sensor; fluidMAG-CT SPIONs used as magnetic labels	SPION suspension; SPION-labeled fibroblasts embedded in alginate–gelatin matrix	Motion-modulated magnetic-susceptibility particle mapping with inverse reconstruction	20 μg SPIONs in 200 mm^3; sensor noise floor ≈500 pT $Hz^{-1}/^2$; spatial resolution: few mm	Experimental cell-label detection demonstrated; molecular/analyte selectivity not evaluated	[80]
Distance-dependent magnetic nanoparticle detection: Fe_3O_4–chitosan fluid	No biospecific ligand; magnetic-particle detection	Related ME device: Metglas/PZT laminate magnetic sensor	Fe_3O_4–chitosan nanoparticle fluid/localized particle spot	Detection of the magnetic stray field from magnetized nanoparticles	2.7×10^{-7} emu; 0.31 μg detectable at 2 mm; ≈50 μg required at 7.6 mm	No biospecific selectivity demonstrated; signal depends strongly on particle amount and sensor distance	[81]
Colored magnetic-particle mapping: distinction of CT100 and ARA100 particle types	No ligand; discrimination based on particle magnetic response	Related ME device: thin-film ME sensor combined with magnetic-particle characterization and PGD reconstruction	Magnetic-particle suspensions in the mapping setup	Higher-harmonic ME detection; amplitude used for spatial distribution and phase for particle-type discrimination	NR	Average phase difference ≈14° between CT100 and ARA100, enabling particle-type discrimination in the proof-of-concept experiment	[82]
Adaptive magnetic-particle mapping: reconstruction of MNP spatial distribution under model uncertainty	No ligand; algorithmic reconstruction rather than biospecific recognition	Related ME device: resonant thin-film ME sensor with adaptive inversion/blind-deconvolution model	Experimental MNP mapping data and simulated/model distributions	Higher-harmonic MNP detection with simultaneous estimation of particle distribution and uncertain sensor/model parameters	NR	Improves reconstruction robustness when the ME-sensor sensitivity axis or magnetic-moment direction is uncertain; not an analyte-selectivity study	[83]

Table 4. *Cont.*

Configuration/Target or Analyte	Recognition Ligand/Labeling Strategy	MENP or ME Platform	Sample Matrix	Detection Principle	LOD/Detection Threshold	Selectivity/Discrimination	Ref.
Magnetic preconcentration and rapid quantification of trapped magnetic nanoparticle–drug conjugate	Magnetophoretic trapping; no biospecific recognition ligand specified for sensing	Related hybrid ME device: integrated piezoelectric/ferromagnetic bilayer ME sensor with magnetic microfluidics	On-chip trapped magnetic nanoparticle–drug conjugate at the microfluidic outlet	IR-induced pyroelectric-current readout after magnetic trapping	Formal LOD NR; response time < 2 s	Concentration-dependent discrimination demonstrated; chemical/analyte selectivity not established by the sensing mechanism	[84]
B. Theoretical or computational MENP sensing concepts							
Converse-ME neural recording: local membrane or extracellular electric potential	No ligand; interaction with local bioelectric field	True core–shell MENP concept used as a local transducer	Neural-tissue/membrane-associated conceptual setting	Biological electric field modifies polarization/strain and magnetic state; remote magnetic readout	NR; projected rather than experimentally established	Spatial localization may arise from membrane association, but biospecific selectivity is not established	[76]
Resonant biomagnetic sensing: weak neural magnetic activity	No ligand; direct interaction with biomagnetic field	Resonant true core–shell MENP sensing concept	Computational neural-source/particle-distribution model	Resonant or field-dependent response of MENPs to weak neural magnetic fields	Computational proof of concept; analytical LOD not experimentally established	Signal discrimination depends on resonance, modulation, lock-in detection, particle distribution, and background-noise rejection	[79]

In a label-free MENP sensor, the target binds directly to the active particle and changes its transduction. This configuration is compact but vulnerable to drift and nonspecific surface changes. In a labeled assay, MENPs bind to a captured target and are detected magnetically or electrically. Labeling increases specificity and allows magnetic preconcentration, but the assay requires additional reagents and washing. A sandwich format is likely to be the most practical near-term route: a capture surface provides selectivity, while functionalized MENPs provide a magnetic and ME-amplified label. Multiplexing can be achieved through particles with different coercivities, resonance frequencies, optical codes, or surface ligands. However, materials encoding must not alter biocompatibility or coupling. A mixture of ferrites with distinct magnetic signatures could support frequency-selective readout, but overlapping relaxation spectra and batch variability may complicate decoding.

6. Biomedical and Bioelectronic Applications

6.1. Drug Delivery, Cancer Therapy, and Immunomodulation

Drug loading onto magnetoelectric nanoparticles can be achieved through electrostatic adsorption, pore loading, covalent conjugation, or encapsulation within an additional polymeric or porous outer layer. The selected strategy must provide sufficiently stable drug retention during circulation while allowing rapid and controllable release after the particles reach the target tissue. In addition, the functional coating should not severely attenuate interfacial strain transfer, field-induced polarization, or the electrical interaction between the active magnetoelectric surface and the surrounding biological environment.

A representative conjugation strategy for CFO-$BaTiO_3$ nanorods is reported by Mushtag et al. [85]. In this approach, the initially hydrophobic nanoparticle surface is coated with an amphiphilic polymer, such as PMA, which introduces accessible carboxyl groups and improves dispersibility in aqueous media. The carboxyl groups are subsequently activated using carbodiimide chemistry, allowing EDC-mediated coupling with amine-containing drug molecules such as doxorubicin (DOX) and methotrexate (MTX). The resulting amide linkage provides more stable loading than simple physical adsorption, while the polymer coating supplies additional sites for drug attachment and potential biomolecular functionalization. Nevertheless, polymer thickness and grafting density must be carefully optimized because an excessively thick or mechanically compliant layer may partially isolate the drug from the active piezoelectric surface and reduce magnetoelectric transduction. The corresponding release profiles demonstrate that drug liberation depends on both the applied magnetic-field amplitude and the exposure duration [86]. At low field amplitudes and short exposure times, only a limited fraction of the loaded DOX or MTX is released. Increasing either the magnetic-field strength or the stimulation time produces a marked increase in the released fraction, with the response approaching saturation under the highest investigated field and time conditions. In the reported CFO-$BaTiO_3$ nanorod system, approximately complete release was approached at magnetic fields of about 4 mT when the exposure was extended to approximately 20–60 min [85]. These results show that the externally applied field can serve not only as an on/off stimulus but also as a means of controlling the release rate and total delivered dose. The proposed mechanism involves magnetic-field-induced changes in the polarization and surface-charge distribution of the magnetoelectric carrier. Magnetostriction of the CFO component transfers strain to the $BaTiO_3$ phase, producing an electrical response at the particle surface. This response can modify electrostatic interactions between the carrier, the polymer coating, and the conjugated drug molecules. Repeated or alternating polarization may weaken drug–carrier interactions, promote deformation or rearrangement of the organic coating, and facilitate diffusion of the therapeutic molecule into the surrounding medium. However, the relative contributions of direct electrostatic

modulation, mechanically assisted desorption, coating deformation, and local heating have not yet been fully separated.

Mahdikia et al. developed [87] plasma-polymer-functionalized $MnFe_2O_4$@$BaTiO_3$ core–shell magnetoelectric nanoparticles for magnetically controlled doxorubicin delivery. As illustrated in Figure 5, the $BaTiO_3$ shell was coated with an acrylic-acid-based plasma polymer, providing surface functional groups for drug conjugation. The combined Ar and acrylic acid/O_2 plasma treatment produced the highest doxorubicin-loading efficiency. Drug-release measurements at 37 °C and pH 7.4 further showed that the cumulative DOX release increased under an applied magnetic field and continued to rise during repeated magnetic-field exposure periods, whereas substantially lower release was observed in the absence of the field. These results demonstrate that surface-functionalized magnetoelectric nanoparticles can combine enhanced drug loading with externally controlled release.

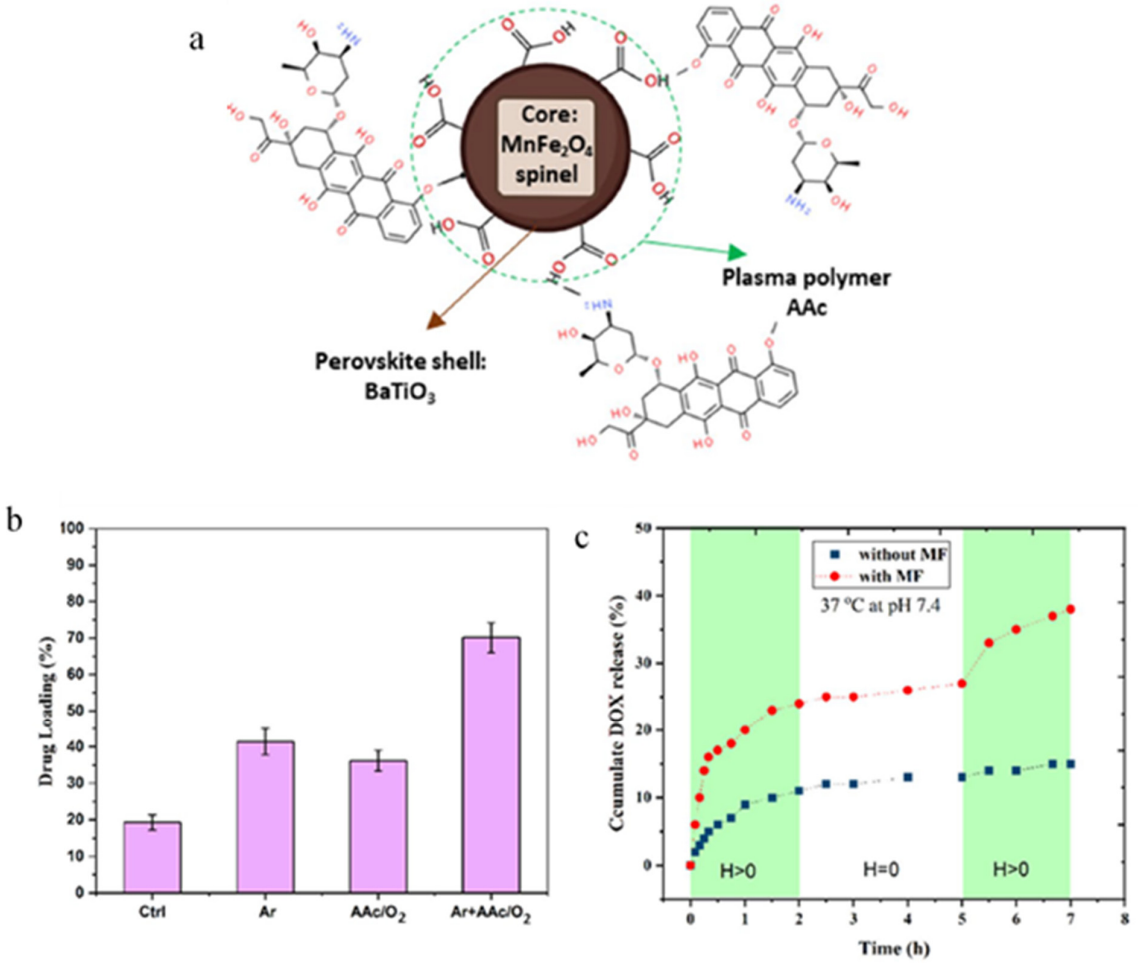


Figure 5. Surface functionalization, doxorubicin loading, and magnetic-field-controlled drug release from $MnFe_2O_4$@$BaTiO_3$ core–shell magnetoelectric nanoparticles. (**a**) Schematic representation of the $MnFe_2O_4$ core, $BaTiO_3$ shell, and acrylic-acid-based plasma-polymer coating used for DOX conjugation. (**b**) Drug-loading efficiency following different plasma-treatment conditions. (**c**) Cumulative DOX release at 37 °C and pH 7.4 in the absence and presence of an applied magnetic field. Adapted from Ref. [87] under the CC BY 4.0 license.

A broader two-stage model for targeted delivery and intracellular release is illustrated in Figure 6. In the first stage, paclitaxel-loaded magnetoelectric nanoparticles are introduced into the circulatory system and guided toward the tumor region using a spatially localized DC magnetic field. In addition to magnetic localization, the applied field polarizes the magnetoelectric nanoparticles and modifies their surface charge. The resulting electrostatic

interaction was proposed to enhance movement of the particles toward malignant cells, particularly when the electrical conductivity of the cancer-cell membrane is transiently increased [86]. When the particles approach the tumor-cell membrane, a sufficiently strong DC magnetic field may promote selective membrane permeabilization or nanoelectroporation and thereby facilitate nanoparticle internalization. In the model proposed by Rodzinski et al. [86], the operating field was selected to exceed the nanoelectroporation threshold of cancer cells while remaining below the corresponding threshold of normal cells. After cellular uptake, a low-frequency AC magnetic field—approximately 50 Oe at 100 Hz in the reported study—was applied to stimulate intracellular release of paclitaxel from the magnetoelectric carriers. This sequential use of a DC field for localization and cellular entry, followed by an AC field for release, provides an attractive strategy for separating targeting from therapeutic activation.

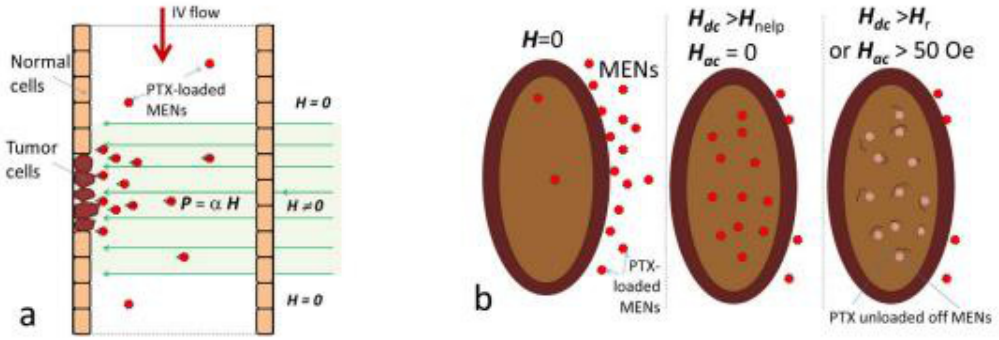


Figure 6. Proposed two-stage mechanism for magnetic-field-controlled targeting, cellular uptake, and intracellular drug release using paclitaxel-loaded magnetoelectric nanoparticles. (**a**) A localized DC magnetic field concentrates the particles within the tumor region and induces magnetoelectric polarization and surface-charge modulation. (**b**) After approaching the cancer-cell membrane, field-assisted nanoelectroporation promotes cellular internalization; subsequent application of a low-frequency AC magnetic field triggers intracellular paclitaxel release. The operating field is proposed to exceed the nanoelectroporation threshold of malignant cells while remaining below that of normal cells. Adapted from Ref. [86].

The same general concept has been extended from paclitaxel to doxorubicin, methotrexate, and antitumor peptides. Early work with approximately 30 nm functionalized CFO–$BaTiO_3$ nanoparticles established magnetic-field-controlled paclitaxel release [88]. Subsequent studies demonstrated targeted anticancer delivery and the transport of antitumor peptides into glioblastoma cells [86,89]. Polymer-coated CFO-$BaTiO_3$ core–shell nanoparticles carrying DOX or MTX also exhibited rapid field-stimulated release and enhanced cytotoxicity toward cancer cells, whereas the corresponding unloaded carriers showed substantially lower toxicity under the reported experimental conditions [85,90]. Despite these promising findings, field-dependent release alone does not unambiguously demonstrate a strain-mediated magnetoelectric mechanism. Magnetic torque, particle vibration, local heating, polymer swelling, pH changes, and nonspecific desorption may produce similar release profiles. Mechanistic studies should therefore include magnetic-only nanoparticles, piezoelectric-only particles, nonmagnetoelectric core–shell controls, field-exposed free drug, and temperature-matched samples. Release experiments should also report the complete magnetic-field waveform, frequency, amplitude, exposure time, duty cycle, sample temperature, pH, ionic strength, particle concentration, hydrodynamic size, drug-loading efficiency, and released drug mass normalized to both the initially loaded drug and nanoparticle mass.

Such controls are essential for distinguishing genuine magnetoelectric release from thermal or mechanically induced drug liberation. A recent overview of CFO–BTO sys-

tems emphasizes the combined roles of magnetic guidance, surface functionalization, and field-triggered release in optimized drug delivery [91]. MENPs offer three complementary capabilities for drug delivery: magnetic guidance, high-surface-area loading, and field-triggered release. CFO-$BaTiO_3$ nanorods loaded with doxorubicin or methotrexate demonstrated rapid release under magnetic stimulation and enhanced cytotoxicity in cancer-cell and spheroid models [85]. Magnetoelectric-silica particles combined MRI contrast, fluorescence, and on-demand doxorubicin delivery [54]. These multifunctional systems can reduce premature release and provide spatially localized treatment. Cancer targeting may be improved through antibodies, peptides, membrane coatings, or physical interactions with the electrical properties of malignant cells [62,63]. Gel-based formulations can retain particles at a surgical site and prolong therapy, as explored for postoperative glioma recurrence [64]. However, a therapeutically effective response must be separated from cobalt-ion toxicity, reactive oxygen species, magnetic heating, and conventional drug action. Studies should report the amount of released drug, intracellular concentration, field-only toxicity, particle-only toxicity, and off-target effects in normal tissue.

The use of MENPs for immunomodulation represents a major conceptual expansion. Dendritic-cell-membrane-coated CFO-$BiFeO_3$ particles were used to target CD4+ T cells and promote a TAF9B-dependent T-helper-2 response under magnetic stimulation, reducing inflammation in murine colitis and arthritis models [66]. This work indicates that localized electrical effects may influence protein synthesis and transcriptional programs, not only membrane excitability. It also shows the value of biologically derived coatings for cell-specific targeting. Extracellular-vesicle-based magnetoelectric therapeutics have been proposed for latency-targeting strategies in HIV [65]. Such approaches could combine tissue homing, cargo delivery, and field-triggered activation. Their complexity is substantial: vesicle composition, donor-cell source, cargo loading, immune recognition, storage, and reproducibility all become critical quality attributes. Nonetheless, biomimetic MENPs may be particularly useful when the biological target is distributed and difficult to reach with conventional electrodes.

6.2. Wireless Neural Stimulation and Brain–Computer Interfaces

Wireless neural stimulation represents one of the most advanced and potentially transformative biomedical applications of magnetoelectric nanoparticles. The central objective is to replace or complement conventional wired electrodes with nanoscale transducers capable of converting externally applied magnetic fields into localized electrical stimuli within neural tissue. In a strain-mediated core–shell MENP, the magnetic field produces magnetostrictive deformation of the magnetic component, which is mechanically transferred to the piezoelectric or ferroelectric phase. The resulting polarization change generates a local electric field that can modify the transmembrane potential, influence voltage-gated ion channels, and stimulate or suppress neuronal activity.

An early conceptual framework for MENP-mediated brain stimulation is studied by Guduru et al. [92]. Following systemic administration, magnetoelectric nanoparticles may be transported across the blood–brain barrier and guided toward selected brain regions using spatially controlled DC magnetic-field gradients. Once the particles are localized within the desired neural region, a low-amplitude AC magnetic field can activate their direct magnetoelectric response and generate local electrical stimulation without requiring implanted conductive leads. The use of magnetic-field gradients for particle localization and AC fields for functional activation provides separate control over targeting and stimulation. The effectiveness of this approach depends not only on the number of particles delivered to the brain but also on their spatial distribution and proximity to excitable cell membranes. The electric field generated by an individual nanoparticle decreases rapidly with distance and

is strongly influenced by particle orientation, aggregation, membrane-binding geometry, ionic screening, and the electrical properties of the extracellular medium. Therefore, a high total particle concentration does not necessarily guarantee effective stimulation if most particles remain distant from neuronal membranes or become confined within mechanically or electrically unfavorable environments. Initial in vivo studies provided proof of concept that CFO-BTO MENPs could modulate electrophysiological activity under external magnetic excitation [92]. Subsequent work demonstrated targeted delivery of intravenously administered MENPs to selected brain regions and reported neuronal activation under magnetic stimulation without detectable neuroinflammation under the tested experimental conditions [92]. These studies established an important connection between nanoparticle delivery, magnetic-field application, local magnetoelectric transduction, and system-level neural activity. Beyond unidirectional stimulation, MENPs have also been proposed as functional elements of a bidirectional wireless brain–computer interface.

Also, Kim et al. [93] demonstrated in vivo wireless neuromodulation using Fe_3O_4–CFO-BTO magnetoelectric nanodiscs injected into the ventral tegmental area (VTA) of mice. As illustrated in Figure 7, the animal was positioned within an alternating magnetic-field coil while a ring-shaped permanent magnet supplied a static offset magnetic field. The combined offset magnetic field and alternating magnetic field activated the magnetoelectric nanodiscs in the VTA, leading to neuronal activation not only at the injection site but also in functionally connected regions, including the nucleus accumbens and medial prefrontal cortex. This experimental configuration demonstrates the potential of magnetoelectric nanostructures for wireless stimulation of deep-brain circuits without implanted stimulation electrodes.

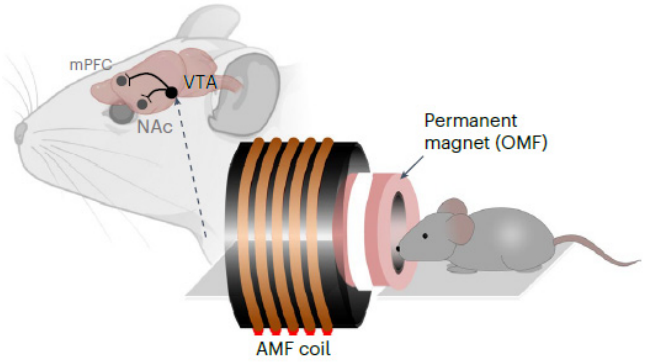


Figure 7. Experimental arrangement for in vivo wireless neuromodulation using magnetoelectric nanodiscs. Magnetoelectric nanodiscs were injected into the ventral tegmental area of the mouse brain. A ring-shaped permanent magnet generated the offset magnetic field, while the surrounding solenoid coil supplied the alternating magnetic field required for magnetoelectric activation. Neural responses were evaluated in the VTA and its connected regions, including the nucleus accumbens and medial prefrontal cortex. Adapted from Ref. [93] under the CC BY 4.0 license.

The two complementary operating modes are illustrated in Figure 8. In the neuromodulation mode, the direct magnetoelectric effect converts an externally applied magnetic field into a localized electric field near the neuronal membrane. This field can modulate ion-channel activity and alter neuronal firing. In the recording mode, the process is reversed: the electric field associated with neuronal activity modifies the polarization and strain state of the piezoelectric phase, which in turn perturbs the magnetization of the magnetic component through converse magnetoelectric coupling and the inverse magnetostrictive response. In the proposed active-recording configuration, a weak AC magnetic field may be used to establish a synchronized magnetic reference response from membrane-associated MENPs. When a nearby neuron fires, the transient membrane electric field perturbs this reference

state, producing a small change in the magnetic response of the particles. In principle, this perturbation could be detected externally using a sufficiently sensitive magnetometer. Such a system would provide a pathway toward wireless stimulation and recording using the same nanoscale transducer platform [76].

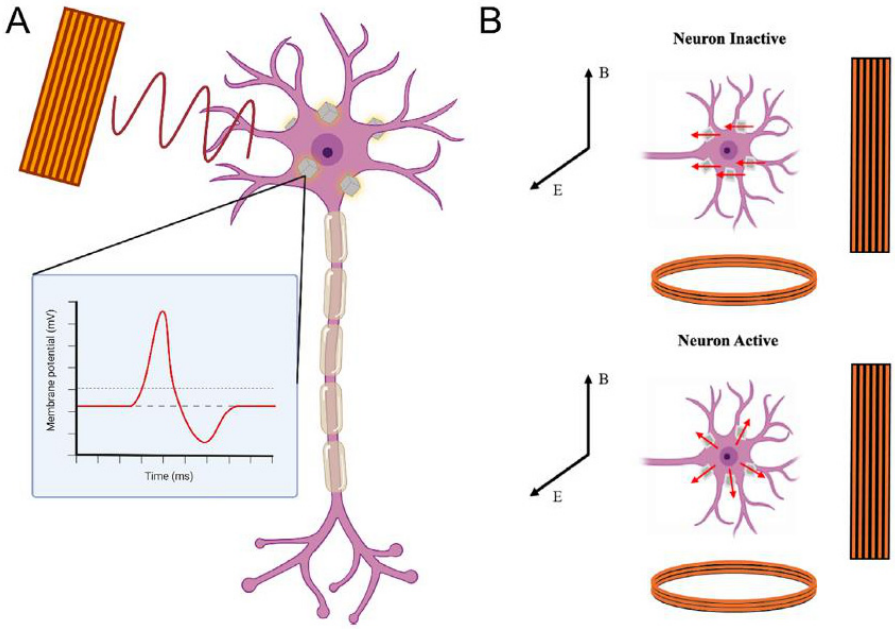


Figure 8. Bidirectional brain–computer interface based on membrane-associated magnetoelectric nanoparticles. (**A**) In the neuromodulation mode, an externally applied magnetic field generates a localized electric field through the direct magnetoelectric effect, thereby modulating neuronal ion channels, membrane potential, and neural activity. (**B**) In the active recording mode, the electric field generated during neuronal firing alters the polarization and strain state of the MENP and consequently perturbs the magnetization of its magnetic component through converse magnetoelectric coupling, allowing the neural event to be detected by an external magnetic-field sensor. Adapted from Ref. [76] under the CC BY license.

The current review identifies this recording concept as scientifically attractive but substantially less experimentally mature than MENP-mediated neuromodulation. The stimulation and recording functions impose different design requirements. Neuromodulation requires a sufficiently large local electric field under biologically acceptable magnetic-field conditions, whereas recording requires detection of extremely small magnetization changes against environmental and physiological magnetic backgrounds. Recording performance is therefore limited by weak neural source fields, random particle orientation, tissue attenuation, particle motion, aggregation, and magnetic signals from particles that are not directly associated with the active neurons. Membrane-specific functionalization, controlled particle orientation, differential magnetic detection, and high-sensitivity field sensors will be required before converse-ME neural recording can be demonstrated convincingly. Recent studies have extended MENP-enabled neural stimulation from general proof-of-concept experiments to disease-oriented therapeutic platforms. Lead-free CFO–BCZT core–shell nanoparticles have demonstrated magnetoelectric performance and favorable biological responses in in vitro and ex vivo nervous-tissue electrostimulation models [53].

Of particular relevance is the biomimetic CFO-BTO platform developed for Parkinson's disease therapy by Zhang et al. [67]. In this study, the magnetoelectric particles were combined with a biologically functional outer coating to improve blood–brain barrier penetration, magnetic targeting, and localization within the diseased neural microenvironment [67]. Following accumulation in the targeted brain region, external magnetic

stimulation can perform more than one therapeutic function. Magnetoelectric activation generates localized electrical cues that may support neuronal activation and differentiation, while field-responsive carrier components can simultaneously promote controlled therapeutic release. The combined strategy therefore integrates magnetic targeting, drug delivery, and wireless electrical stimulation within a single multifunctional platform. In the Parkinson's disease model, this approach was reported to promote neural differentiation and reverse damage to dopaminergic neurons [67].

Related in vivo work has reported mitigation of motor deficits in Parkinsonian mice using MENP-mediated stimulation and provided evidence that the particles can retain functional activity in brain tissue over extended periods [94]. These findings strengthen the translational relevance of MENP-based neuromodulation by moving beyond short-term electrophysiological activation toward disease-related behavioral outcomes. Nevertheless, clinically meaningful interpretation requires standardized reporting of particle dose, biodistribution, stimulation waveform, field amplitude, frequency, duty cycle, treatment duration, tissue temperature, behavioral endpoints, and long-term histological response. Several alternative wireless neural-stimulation technologies provide useful performance benchmarks. Injectable nanoelectrodes have enabled wireless deep-brain stimulation in freely moving mice, while miniaturized magnetoelectric structures have delivered therapeutic-frequency stimulation in Parkinsonian animal models [95,96]. However, such systems should be distinguished from freely dispersed core–shell MENPs because their dimensions, implantation procedures, resonance behavior, power-transfer mechanisms, and tissue interfaces differ substantially. Despite the encouraging results, the mechanism of MENP-mediated neural activation must be examined carefully.

Dominguez-Paredes et al. [94] evaluated magnetoelectric nanoparticle-mediated wireless deep-brain stimulation in a 6-hydroxydopamine-induced mouse model of Parkinson's disease. As illustrated in Figure 9, MENPs or control magnetic nanoparticles were stereotactically administered, followed by a two-week recovery period and five sequential magnetic-stimulation blocks. The stimulation protocol systematically varied the alternating magnetic-field frequency and amplitude, while locomotor and motor-coordination outcomes were assessed using CatWalk, open-field, and RotaRod tests. During each behavioral session, mice were placed inside a Helmholtz-coil system and exposed to magnetic stimulation for 3 min. This experimental design enabled direct assessment of the influence of magnetic-field parameters on MENP-mediated neuromodulation and motor recovery in Parkinsonian mice.

Magnetic torque, particle displacement, mechanical membrane perturbation, local heating, and indirect biological responses can occur simultaneously with strain-mediated magnetoelectric transduction. Appropriate controls should therefore include magnetic-only nanoparticles, piezoelectric-only particles, nonmagnetoelectric core–shell structures, particle-free magnetic-field exposure, temperature-matched samples, and pharmacological inhibition of the relevant ion channels. Direct measurement or realistic modeling of the local electric field in physiological media is also essential. The long-term objective is a closed-loop MENP-enabled brain–computer interface in which neural signals are recorded, decoded, and used to adapt subsequent stimulation. Achieving this goal will require precise control of particle location, orientation, membrane association, persistence, and clearance, together with highly sensitive magnetic readout and robust signal-processing methods. Thus, wireless MENP-mediated neuromodulation has reached convincing proof-of-concept and early disease-model validation, whereas bidirectional recording remains an important but largely prospective technological pathway.

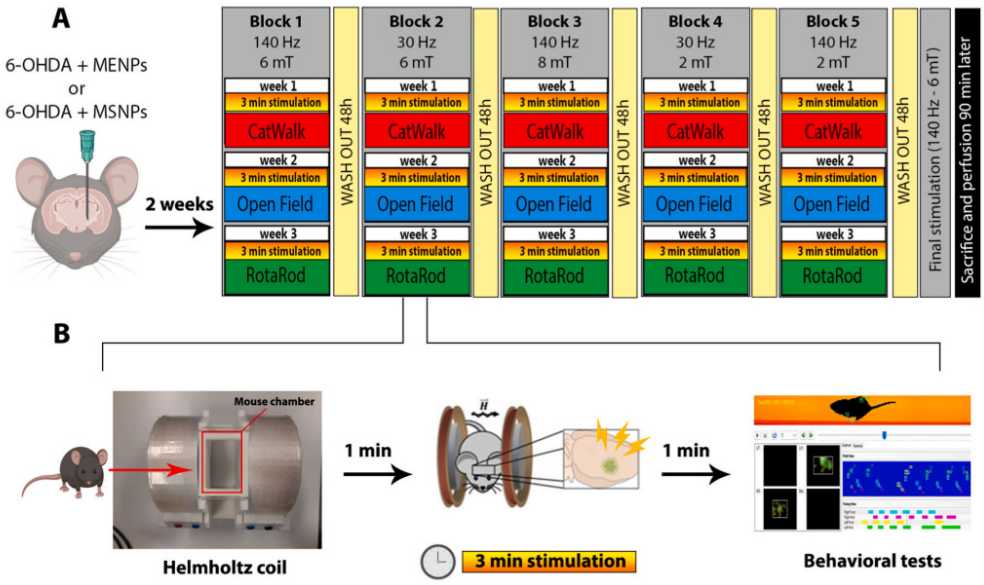


Figure 9. Experimental protocol for magnetoelectric nanoparticle-mediated wireless deep-brain stimulation in a Parkinsonian mouse model. (**A**) Following intracranial administration of MENPs or control magnetic nanoparticles in 6-OHDA-lesioned mice, five stimulation blocks with different alternating magnetic-field frequencies and amplitudes were applied. Motor performance was evaluated longitudinally using CatWalk, open-field, and RotaRod tests. (**B**) During stimulation, each mouse was positioned within a Helmholtz-coil system, exposed to the magnetic field for 3 min, and subsequently subjected to behavioral testing. Adapted from Ref. [94] under the CC BY 4.0 license.

6.3. Tissue Engineering, Wound Healing, and Multimodal Systems

Embedding MENPs in a scaffold can transform a local biomaterial into a wirelessly active tissue-engineering platform. A flexible, biodegradable magnetoelectric paper has been developed for in situ personalization of bioelectric implants [97]. Such macroscopic devices illustrate how active magnetic and piezoelectric components can be combined with biodegradable substrates, although their architecture differs from injectable core–shell particles. Wearable hybrid energy harvesters based on core–shell ME nanoparticles similarly demonstrate integration with flexible conductive polymers for biomedical power and sensing [98]. Three-dimensional GelMA hydrogels containing CFO-$BiFeO_3$ particles have enabled wireless electrical stimulation of cardiac cells [99]. The hydrogel provided a soft, porous environment, while magnetic stimulation improved cell viability, proliferation, and organization relative to unstimulated controls. This is a strong example of hierarchical design: the nanoparticle supplies transduction, and the hydrogel supplies tissue-like mechanics. The study also underscores a common limitation: biological improvement can be demonstrated even when the absolute local ME coefficient in the hydrated scaffold is not directly measured.

Future work should correlate field, particle loading, local potential, scaffold mechanics, and electrophysiological outcome. Electrospun PVDF-TrFE-$CoFe_2O_4$ fibers have been developed for wound-healing applications [100]. Fibrous scaffolds can mimic the extracellular matrix, promote polymer chain orientation, and distribute magnetic particles over a large area. A field-responsive scaffold could provide intermittent electrical cues without implanted electrodes. The main challenges are sterilization, mechanical fatigue, particle release, and ensuring that the field exposure does not cause harmful heating in an open wound. The biological rationale for these scaffolds is supported by the broader electrotherapy literature. Electrical and pulsed-electromagnetic stimulation can influence cell migration, angiogenesis, fibroblast activity, extracellular-matrix deposition, and inflammatory signaling during tissue repair [101]. In infected burn models, pulsed high-voltage

electric fields have also been investigated as a nonpharmacological method for reducing persistent Pseudomonas aeruginosa infection [102]. MENP-loaded scaffolds could, in principle, provide part of this electrical functionality without direct wired contact, but the local waveform at the wound surface must be measured rather than inferred from the applied magnetic field.

Non-ME nanofibrous and nanoparticle-containing wound materials provide useful biological comparators. Electrospun silk-fibroin matrices and succinyl-chitosan nanoparticle films have shown wound-repair activity in preclinical models [103,104], while standardized experimental wound models emphasize the need for quantitative assessment of closure, re-epithelialization, collagen organization, vascularization, inflammation, and tensile recovery [105]. Future magnetoelectric wound studies should include these endpoints together with bacterial burden, pain-related outcomes, particle retention, and histological evidence that the response is attributable to the ME stimulus rather than only to scaffold chemistry.

MENPs can also generate charge for catalytic or redox processes. Catalytic degradation of organic dyes has been linked to antiproliferative effects and illustrates the possibility of magnetically controlled reactive chemistry [106]. In a biomedical context, similar charge generation could be used for localized reactive oxygen species production, antibacterial action, or catalytic prodrug activation. The therapeutic window must be carefully controlled because nonspecific oxidative stress can damage healthy tissue. Theranostic platforms combine therapy and diagnosis. Magnetic cores provide MRI contrast or magnetic tracking; fluorescent outer layers provide optical localization; drug cargo provides therapy; and the ME effect provides remote activation. The complexity can be justified if each function contributes independent clinical value. Otherwise, multifunctionality may increase manufacturing and regulatory burden without improving outcome. A modular approach, in which a validated ME core–shell platform receives application-specific outer coatings, is likely to be more scalable than developing a completely new composition for every disease.

At larger device scales, ME materials can serve as antennas and wireless power links. Bio-integrated microrobotic systems with overtone ultrawideband ME antennas have demonstrated the broader potential of acoustic-mode ME structures for wireless telemetry [107]. Although these are not nanoparticle biosensors, they define a complementary pathway: MENPs may interact with cells locally, while integrated ME antennas provide communication and power transfer at the device level. Future implants could combine both scales, using an ME antenna to generate a controlled magnetic field for an internal MENP-loaded scaffold. The choice between dispersed particles and an integrated ME implant depends on the application. Freely distributed particles offer cellular-scale access but are difficult to retrieve and calibrate. Immobilized particles in a scaffold or implant provide reproducible geometry and containment but require implantation. Hybrid strategies—injectable gels, biodegradable patches, or magnetically retained depots—may offer the most practical compromise. Earlier implant studies demonstrate why ME coupling is attractive for deeply positioned devices.

The NanoNeuroRFID concept integrated miniaturized ME antennas for wireless communication and power transfer, while encapsulated ME composites and system-level power-transfer studies examined the effects of field nonuniformity, alignment, and orientation in biomedical implants [108–110]. These findings are directly relevant to MENP systems because the external coil and field geometry ultimately determine both the usable actuation volume and the safety margin. An integrated implant can provide reproducible geometry, whereas dispersed particles provide cellular access; hybrid devices may use a larger ME receiver to power or coordinate a localized MENP-containing interface. Representative biomedical and bioelectronic applications are summarized in Table 5, highlighting the platforms used, experimentally demonstrated outcomes, and key remaining challenges.

The comparison also illustrates the progression of the field from proof-of-concept studies toward in vivo and potentially translational applications.

Table 5. Representative biomedical applications and evidence level.

Application	Representative Platform	Demonstrated Outcome	Key Remaining Question
Neural stimulation	CFO–BCZT true core–shell particles	In vitro and ex vivo nervous-tissue electrostimulation [53]	Quantitative local field and chronic in vivo dose
Parkinson's disease	Biomimetic $BaTiO_3$–$CoFe_2O_4$ carrier, core–shell-derived system	Drug delivery, neuronal activation, and functional improvement [67]	Long-term biodistribution and scalable targeting
Wireless deep-brain stimulation	MENPs in Parkinsonian mice, MEN platform	Motor-deficit mitigation and persistent efficacy [94]	Human-scale excitation and safety
Cancer drug delivery	True CFO-$BaTiO_3$ nanorods	Field-triggered drug release and enhanced cytotoxicity [85]	Mechanism-specific controls and systemic pharmacokinetics
Multimodal cancer theranostics	Magnetoelectric–silica particles, core–shell-derived system	MRI/fluorescence tracking and doxorubicin delivery [54]	Validation of ME mechanism and in vivo clearance
Immunomodulation	Cell-membrane-coated CFO-$BiFeO_3$, core–shell-derived system	T-helper-2 expansion and reduced inflammation [66]	Manufacturing consistency and immune safety
Cardiac tissue engineering	CFO-$BiFeO_3$ in GelMA, core–shell-derived system	Wireless stimulation and improved cell growth [99]	Electrophysiological maturation and in vivo integration
Wound healing	PVDF-TrFE-$CoFe_2O_4$ fibers, ME composite scaffold	Electroactive field-responsive scaffold [100]	Sterilization, particle retention, and clinical efficacy
Biodegradable implants	Flexible ME paper	Personalizable wireless bioelectric interface [97]	Degradation products and lifetime control
Catalytic therapy	MENP-mediated dye degradation, MEN platform	Field-responsive catalytic and antiproliferative effects [106]	Selectivity for diseased tissue
Early field-triggered drug release	Functionalized true CFO–BTO MENPs	Paclitaxel release under magnetic control [88]	Reproducibility in physiological media and mechanism-specific controls
Targeted anticancer delivery	Functionalized true CFO–BTO and peptide/drug-loaded MENPs	Targeted release and delivery to cancer models [86,89,90]	Pharmacokinetics, clearance, and healthy-tissue controls
Early in vivo brain stimulation	True CFO–BTO MENPs	Electrophysiological and cortical activity modulation [92,111]	Particle dosimetry, localization, and chronic neuroinflammation
Wireless implant powering	Miniaturized ME antennas and encapsulated composites	Wireless energy transfer and neural-interface concepts [108–110]	Alignment tolerance, tissue-scale efficiency, and system integration

7. Biological Safety

The biological safety of magnetoelectric nanoparticles should be evaluated for the complete field-exposed formulation rather than inferred solely from the nominal composi-

tion of the magnetic core or piezoelectric/ferroelectric shell. Safety depends on particle size, hydrodynamic diameter, surface charge, aggregation state, coating chemistry, administered dose, exposure duration, and route of administration. In biological fluids, adsorption of proteins forms a dynamic protein corona that can alter colloidal stability, cellular uptake, immune recognition, biodistribution, and clearance. Therefore, particle stability and surface properties should be characterized in serum-containing and other physiologically relevant media rather than only in water or simple buffers.

Dose and cumulative exposure are particularly important considerations. Safety studies should report particle concentration, administered mass, route of administration, treatment frequency, and cumulative dose. For magnetically targeted systems, the local particle concentration may substantially exceed the nominal systemic concentration because particles can accumulate within the target region. Moreover, the same administered dose may produce different biological effects depending on whether particles remain extracellular, bind to cell membranes, or are internalized into endosomal or lysosomal compartments. Dose-dependent evaluation should therefore extend beyond short-term cell viability to include oxidative stress, inflammatory signaling, membrane damage, and, where appropriate, genotoxicity.

Composition-specific risks are especially relevant for Co-, Ni-, Bi-, and Pb-containing phases because degradation may result in the release of biologically active ions. Cobalt ferrite, for example, offers attractive magnetic and magnetostrictive properties but can undergo partial intracellular degradation under acidic lysosomal conditions, raising concerns regarding Co-ion release and long-term persistence. Similar considerations apply to Ni- and Bi-containing systems. $BaTiO_3$ is generally more attractive for biomedical applications because it is lead-free, but its safety remains dependent on particle size, concentration, surface chemistry, and exposure time. PZT-containing systems require particular caution because degradation or damage to the protective coating could expose Pb-containing material. For such systems, long-term coating integrity and ion-leaching tests are essential.

For core–shell MENPs, shell degradation under physiological conditions is a particularly important but insufficiently investigated issue. A continuous shell observed in the as-prepared state may undergo dissolution, defect formation, or structural modification following prolonged exposure to physiological salts, proteins, enzymes, or acidic intracellular environments. Partial degradation of the piezoelectric shell could expose the magnetic core, increase ion release, modify aggregation and surface charge, and simultaneously alter interfacial strain transfer and magnetoelectric performance. Consequently, shell integrity, elemental release, particle morphology, and ME functionality should ideally be monitored before and after prolonged incubation in physiologically relevant and lysosome-mimicking media.

Biodistribution, biodegradation, and long-term organ accumulation also require systematic investigation. Following systemic administration, nanoparticles may accumulate in the liver, spleen, kidneys, lungs, or other non-target organs, depending on particle size, surface chemistry, and protein-corona formation. Magnetic targeting does not necessarily eliminate this off-target distribution. Biodistribution studies should therefore quantify both target-tissue accumulation and residual particle burden in major organs at multiple time points. Importantly, disappearance of particles from the circulation should not be interpreted as complete clearance, because particles may instead remain within tissue macrophages or intracellular compartments. Repeated administration is of particular concern when clearance between doses is incomplete, as this may lead to progressive organ accumulation.

Repeated magnetic-field exposure introduces an additional safety consideration specific to MENP-based technologies. Magnetoelectric activation may occur together with

magnetic torque, particle motion, mechanical membrane perturbation, magnetic losses, or local heating. Chronic studies should therefore reproduce the intended operating conditions and report magnetic-field amplitude, frequency, waveform, duty cycle, exposure duration, number of stimulation sessions, and tissue temperature. Appropriate particle-only, field-only, magnetic-only, and temperature-matched controls are needed to distinguish genuine magnetoelectric effects from nonspecific magnetic, mechanical, or thermal responses.

These issues are particularly important for long-term neural, cardiac, and systemic applications, where particles may remain in tissue for extended periods and undergo repeated stimulation. Safety evaluation should therefore include cytotoxicity, hemocompatibility, inflammatory and immune responses, organ distribution, clearance, degradation products, repeated-dose toxicity, and chronic histopathology. Future biomedical translation should prioritize lead-free, biologically stable, biodegradable, or safely clearable MENP systems, while standardized reporting of dose, biodistribution, shell integrity, ion release, repeated-field exposure, and long-term biological outcomes will be essential for establishing realistic safety margins.

8. Future Directions and Conclusions

Future research should prioritize reproducible, lead-free, and biologically stable core–shell systems that generate a quantitatively measurable electrical response under clinically realistic magnetic-field conditions. Standardized reporting of particle size, shell thickness, phase composition, magnetization, piezoresponse, conductivity, colloidal stability, field amplitude, frequency, and measurement geometry is necessary to enable reliable comparison between studies. Measurements should increasingly be performed in physiological media because ionic screening, protein adsorption, aggregation, and particle–cell distance can strongly modify the local electric stimulus.

For biosensing applications, future studies must move beyond proof-of-concept transduction and provide complete analytical validation, including calibration range, sensitivity, selectivity, limit of detection, matrix recovery, reproducibility, storage stability, and comparison with established reference methods. The nanoparticle and the external readout system should be developed together, using approaches such as differential magnetic detection, lock-in amplification, resonance tracking, electrochemical interfaces, or optical reporters.

Closed-loop and bidirectional systems represent an important long-term opportunity. In such platforms, MENPs could sense local biological activity and deliver a controlled therapeutic or stimulatory response. Achieving this goal will require stable localization, artifact-resistant simultaneous sensing and stimulation, accurate dosimetry, patient-specific modeling, and multiscale relationships linking particle structure, magnetic-field exposure, tissue properties, and biological outcome.

Translation will also require reproducible and scalable manufacturing rather than optimization of individual laboratory batches. Batch-to-batch consistency should be demonstrated for critical physicochemical and functional attributes, including core size and size distribution, shell thickness and continuity, phase purity, hydrodynamic size, surface charge, aggregation state, magnetic properties, piezoelectric response, and magnetoelectric output. Scale-up of core–shell synthesis is particularly challenging because changes in mixing, precursor addition, heat and mass transfer, washing, and calcination can modify nucleation, shell coverage, aggregation, and interfacial quality. Accordingly, scale-up should be evaluated by predefined acceptance criteria rather than by nominally reproducing the laboratory synthesis protocol.

Additional translational requirements include validated sterilization, endotoxin control, and storage-stability testing of the final formulation. Sterilization should not compromise shell integrity, surface functionalization, colloidal stability, or ME performance, and

aseptic processing may be necessary when terminal sterilization alters these properties. Storage studies should evaluate aggregation, sedimentation, chemical degradation, ion release, ligand or coating stability, and retention of magnetic and ME functionality over the intended shelf life. For biomedical MENPs, critical quality attributes should therefore connect material structure with biological safety and functional performance, providing measurable specifications for manufacturing consistency and regulatory evaluation.

In conclusion, magnetoelectric core–shell nanoparticles combine magnetic remote addressability with localized electrical transduction in a single nanoscale platform. Ferrite–$BaTiO_3$ systems remain the most established material family, while Fe_3O_4-based cores, lead-free perovskites, polymer composites, and biomimetic coatings are expanding the design space. The core–shell geometry can improve interfacial contact and stress transfer, but performance depends critically on particle size, shell thickness, crystallinity, conductivity, aggregation, and measurement conditions. Direct comparison between studies remains difficult because the reported quantities and experimental configurations are not standardized. The biomedical literature now extends beyond conceptual drug delivery to neural stimulation, Parkinson's disease models, immunomodulation, cardiac tissue engineering, wound healing, and wireless bioelectronics. These advances are encouraging, but many studies still infer the ME mechanism from material composition or biological outcome rather than directly measuring the local electrical stimulus. Reliable progress will require coupled materials characterization, calibrated field exposure, mechanistic controls, and application-specific safety assessment.

The most credible route to translation is therefore not simply to maximize a nominal ME coefficient, but to engineer a reproducible and biocompatible platform that produces a measurable stimulus in the intended biological environment, can be integrated with a practical readout or delivery system, and satisfies manufacturing and regulatory requirements. With standardized measurement, lead-free and biodegradable materials, robust surface functionalization, and rigorous in vivo validation, magnetoelectric core–shell nanoparticles could develop from laboratory demonstrations into useful biosensing, therapeutic, and bioelectronic technologies.

Funding: This study was supported by the Scientific and Technological Research Council of Turkey (TUBITAK) under Grant Number 123M414.

Data Availability Statement: Data will be made available on request.

Acknowledgments: The author thanks TUBITAK for their support.

Conflicts of Interest: The author declares no conflicts of interest.

References

1. Song, H.; Listyawan, M.A.; Ryu, J. Core–Shell Magnetoelectric Nanoparticles: Materials, Synthesis, Magnetoelectricity, and Applications. *Actuators* **2022**, *11*, 380. [CrossRef]
2. Palneedi, H.; Annapureddy, V.; Priya, S.; Ryu, J. Status and Perspectives of Multiferroic Magnetoelectric Composite Materials and Applications. *Actuators* **2016**, *5*, 9. [CrossRef]
3. Kopyl, S.; Surmenev, R.; Surmeneva, M.; Fetisov, Y.; Kholkin, A. Magnetoelectric Effect: Principles and Applications in Biology and Medicine—A Review. *Mater. Today Bio* **2021**, *12*, 100149. [CrossRef] [PubMed]
4. Durmaz, E.; Inan, O.O.; Atalay, S. Fabrication and Characterization of a Vacodur49/PZT/Vacodur49 Magnetoelectric Sensor. *J. Magn. Magn. Mater.* **2025**, *635*, 173623. [CrossRef]
5. Khizroev, S. Technobiology's Enabler: The Magnetoelectric Nanoparticle. *Cold Spring Harb. Perspect. Med.* **2019**, *9*, a034207. [CrossRef] [PubMed]
6. Wang, P.; Zhang, E.; Toledo, D.; Smith, I.T.; Navarrete, B.; Furman, N.; Hernandez, A.F.; Telusma, M.; McDaniel, D.; Liang, P.; et al. Colossal Magnetoelectric Effect in Core–Shell Magnetoelectric Nanoparticles. *Nano Lett.* **2020**, *20*, 5765–5772. [CrossRef] [PubMed]

7. Wang, L.M.; Petracic, O.; Mattauch, S.; Koutsioumbas, A.; Wei, X.-K.; Heggen, M.; Leffler, V.; Ehlert, S.; Brueckel, T. Magnetoelectric coupling in iron oxide nanoparticle—Barium titanate composites. *J. Phys. D Appl. Phys.* **2019**, *52*, 065301. [CrossRef]
8. Kanurin, D.A.; Amirov, A.A.; Liu, N.N.; Nizamov, T.R.; Alekhina, Y.A.; Kritskiy, A.A.; Platonova, I.V.; Perov, N.S.; Tishin, A.M. Local Magnetoelectric Effect in Fe_3O_4–$BaTiO_3$ Nanocomposites. *J. Nanopart. Res.* **2025**, *27*, 113. [CrossRef]
9. Amirov, A.; Kanurin, D.; Darwish, A.; Leesment, S.; Liu, N.; Platonova, I.; He, Q.; Sukhorukov, G.; Tishin, A. Enhanced Local Magnetoelectric Effect in Core–Shell Structured $CoFe_2O_4$–$BaTiO_3$ Nanocomposites. *J. Magn. Magn. Mater.* **2026**, *655*, 174346. [CrossRef]
10. Huong Giang, D.T.; Duc, P.A.; Ngoc, N.T.; Duc, N.H. Geomagnetic Sensors Based on Metglas/PZT Laminates. *Sens. Actuators A Phys.* **2012**, *179*, 78–82. [CrossRef]
11. Pradhan, D.K.; Kumari, S.; Rack, P.D. Magnetoelectric Composites: Applications, Coupling Mechanisms, and Future Directions. *Nanomaterials* **2020**, *10*, 2072. [CrossRef] [PubMed]
12. Shaposhnikova, T.S.; Mamin, R.F. Electric Polarization in Small Magnetic Particles. *J. Surf. Investig.* **2021**, *15*, 1282–1285. [CrossRef]
13. Talleb, H.; Do, T.A.; Gensbittel, A.; Ren, Z. Modeling of Multiferroic Nanoparticle Composites With an Analytical Multiscale Approach. *IEEE Trans. Magn.* **2020**, *56*, 6700504. [CrossRef]
14. Samghabadi, F.S.; Chang, L.; Khodadadi, M.; Martirosyan, K.S.; Litvinov, D. Scalable, cost-efficient synthesis and properties optimization of magnetoelectric cobalt ferrite/barium titanate composites. *APL Mater.* **2021**, *9*, 021104. [CrossRef]
15. Etier, M.; Schmitz-Antoniak, C.; Salamon, S.; Trivedi, H.; Gao, Y.; Nazrabi, A.; Landers, J.; Gautam, D.; Winterer, M.; Schmitz, D.; et al. Magnetoelectric coupling on multiferroic cobalt ferrite-barium titanate ceramic composites with different connectivity schemes. *Acta Mater.* **2015**, *90*, 1–9. [CrossRef]
16. Nayek, C.; Sahoo, K.K.; Murugavel, P. Magnetoelectric effect in $La_{0.7}Sr_{0.3}MnO_3$-$BaTiO_3$ core–shell nanocomposite. *Mater. Res. Bull.* **2013**, *48*, 1308–1311. [CrossRef]
17. Majeed, J.; Jayakumar, O.D.; Salunke, H.G.; Mandal, B.P.; Lawes, G.; Naik, R.; Tyagi, A.K. Multifunctional hybrid structures of ferromagnetic FePt and ferroelectric $BaTiO_3$ nanoparticles: Facile synthesis and characterization. *RSC Adv.* **2013**, *3*, 596–602. [CrossRef]
18. Erdem, D.; Bingham, N.S.; Heiligtag, F.J.; Pilet, N.; Warnicke, P.; Vaz, C.A.F.; Shi, Y.; Buzzi, M.; Rupp, J.L.M.; Heyderman, L.J.; et al. Nanoparticle-Based Magnetoelectric $BaTiO_3$-$CoFe_2O_4$ Thin Film Heterostructures for Voltage Control of Magnetism. *ACS Nano* **2016**, *10*, 9840–9851. [CrossRef] [PubMed]
19. Corral-Flores, V.; Bueno-Baques, D.; Ziolo, R.F. Synthesis and Characterization of Novel $CoFe_2O_4$-$BaTiO_3$ Multiferroic Core–Shell Type Nanostructures. *Acta Mater.* **2010**, *58*, 764–769. [CrossRef]
20. Selvi, M.M.; Manimuthu, P.; Kumar, K.S.; Venkateswaran, C. Magnetodielectric Properties of $CoFe_2O_4$-$BaTiO_3$ Core–Shell Nanocomposite. *J. Magn. Magn. Mater.* **2014**, *369*, 155–161. [CrossRef]
21. Thankachan, R.M.; Raneesh, B.; Mayeen, A.; Karthika, S.; Vivek, S.; Nair, S.S.; Thomas, S.; Kalarikkal, N. Room-Temperature Magnetoelectric Coupling Effect in $CuFe_2O_4$-$BaTiO_3$ Core–Shell and Nanocomposites. *J. Alloys Compd.* **2018**, *731*, 288–296. [CrossRef]
22. Zhou, J.P.; Lv, L.; Liu, Q.; Zhang, Y.X.; Liu, P. Hydrothermal Synthesis and Properties of $NiFe_2O_4$@$BaTiO_3$ Composites with Well-Matched Interface. *Sci. Technol. Adv. Mater.* **2012**, *13*, 045001. [CrossRef] [PubMed]
23. Wang, T.; Bian, X.; Yang, C.; Zhao, S.; Yu, M. Ferrofluids Based on Co-Fe-Si-B Amorphous Nanoparticles. *Appl. Surf. Sci.* **2017**, *399*, 663–669. [CrossRef]
24. Yuan, Z.Z.; Chen, J.M.; Lu, Y.; Chen, X.D. Preparation and Magnetic Properties of Amorphous Co-Zr-B Alloy Nanopowders. *J. Alloys Compd.* **2008**, *450*, 245–251. [CrossRef]
25. Zak, A.K.; Majid, W.H.A. Effect of Solvent on Structure and Optical Properties of PZT Nanoparticles Prepared by Sol-Gel Method in the Infrared Region. *Ceram. Int.* **2011**, *37*, 753–758. [CrossRef]
26. Xie, S.H.; Li, J.Y.; Qiao, Y.; Liu, Y.Y.; Lan, L.N.; Zhou, Y.C.; Tan, S.T. Multiferroic $CoFe_2O_4$-$Pb(Zr_{0.52}Ti_{0.48})O_3$ Nanofibers by Electrospinning. *Appl. Phys. Lett.* **2008**, *92*, 062901. [CrossRef]
27. Amorín, H.; Hungría, T.; Landa-Cánovas, A.R.; Torres, M.; Dollé, M.; Algueró, M.; Castro, A. Nanopowders of ferroic oxides for magnetoelectric composites. *J. Nanoparticle Res.* **2011**, *13*, 4189–4200. [CrossRef]
28. Henkes, A.E.; Bauer, J.C.; Sra, A.K.; Johnson, R.D.; Cable, R.E.; Schaak, R.E. Low-temperature nanoparticle-directed solid-state synthesis of ternary and quaternary transition metal oxides. *Chem. Mater.* **2006**, *18*, 567–571. [CrossRef]
29. Fernández, C.P.; Zabotto, F.L.; Garcia, D.; Kiminami, R.H. In situ sol gel co-synthesis under controlled pH and microwave sintering of PZT/$CoFe_2O_4$ magnetoelectric composite ceramics. *Ceram. Int.* **2016**, *42*, 3239–3249. [CrossRef]
30. Evans, G.; Duong, G.V.; Ingleson, M.J.; Xu, Z.; Jones, J.T.A.; Khimyak, Y.Z.; Claridge, J.B.; Rosseinsky, M.J. Chemical Bonding Assembly of Multifunctional Oxide Nanocomposites. *Adv. Funct. Mater.* **2010**, *20*, 231–238. [CrossRef]
31. Mu, X.J.; Zhang, H.; Zhang, C.; Yang, S.; Huang, Y.; Xu, J.; Zhang, Y.; Li, Q.; Wang, X.; Cao, D.; et al. Poly(vinylidene fluoride-trifluoroethylene)/cobalt ferrite composite films with a self-biased magnetoelectric effect for flexible AC magnetic sensors. *J. Mater. Sci.* **2021**, *56*, 9728–9740. [CrossRef]

32. Martins, P.; Moya, X.; Caparrós, C.; Fernandez, J.; Mathur, N.D.; Lanceros-Mendez, S. Large linear anhysteretic magnetoelectric voltage coefficients in $CoFe_2O_4$/polyvinylidene fluoride 0–3 nanocomposites. *J. Nanoparticle Res.* **2013**, *15*, 1825. [CrossRef]
33. Martins, P.; Gonçalves, R.; Lanceros-Mendez, S.; Lasheras, A.; Gutiérrez, J.; Barandiarán, J. Effect of filler dispersion and dispersion method on the piezoelectric and magnetoelectric response of $CoFe_2O_4$/P(VDF-TrFE) nanocomposites. *Appl. Surf. Sci.* **2014**, *313*, 215–219. [CrossRef]
34. Salnikov, V.D.; Aga-Tagieva, S.E.; Kolesnikova, V.; Tovpinets, A.; Omelyanchik, A.; Rodionova, V. Effect of PEG nanoparticle surface coating on the magnetic and structural properties of $CoFe_2O_4$/PVDF composites. *J. Magn. Magn. Mater.* **2024**, *595*, 171498. [CrossRef]
35. Ben Osman, C.; Nowak, S.; Garcia-Sanchez, A.; Charles, Y.; Ammar, S.; Mercone, S.; Mammeri, F. In situ monitored stretching induced α to β allotropic transformation of flexible poly(vinylidene fluoride)-$CoFe_2O_4$ hybrid films: The role of nanoparticles inclusion. *Eur. Polym. J.* **2016**, *84*, 602–611. [CrossRef]
36. Ourry, L.; Marchesini, S.; Bibani, M.; Mercone, S.; Ammar, S.; Mammeri, F. Influence of nanoparticle size and concentration on the electroactive phase content of PVDF in PVDF-$CoFe_2O_4$-based hybrid films. *Phys. Status Solidi A* **2015**, *212*, 252–258. [CrossRef]
37. Gonçalves, R.; Martins, P.; Correia, D.M.; Sencadas, V.; Vilas, J.L.; León, L.M.; Botelho, G.; Lanceros-Méndez, S. Development of magnetoelectric $CoFe_2O_4$/poly(vinylidene fluoride) microspheres. *RSC Adv.* **2015**, *5*, 35852–35857. [CrossRef]
38. Gonçalves, R.; Martins, P.; Moya, X.; Ghidini, M.; Sencadas, V.; Botelho, G.; Mathur, N.D.; Lanceros-Mendez, S. Magnetoelectric $CoFe_2O_4$/polyvinylidene fluoride electrospun nanofibres. *Nanoscale* **2015**, *7*, 8058–8061. [CrossRef] [PubMed]
39. Martins, P.; Costa, C.M.; Benelmekki, M.; Lanceros-Mendez, S. Preparation of Magnetoelectric Composites by Nucleation of the Electroactive β-Phase of Poly(vinylidene fluoride) by $NiZnFe_2O_4$ Nanoparticles. *Sens. Lett.* **2013**, *11*, 110–114. [CrossRef]
40. Barrera, G.; Allia, P.; Tiberto, P. Exploring strategies for enhancing magnetoelectric effects in piezoelectric polymer-magnetostrictive nanoparticle systems. *J. Alloys Compd.* **2025**, *1047*, 184832. [CrossRef]
41. Wang, C.Y.; Xu, L.F.; Lv, X.; Ge, Y.; Wang, R.; Liang, S.; Xiao, H.; Yang, C. Retainable large magnetoelectric coupling in $BiFeO_3$@$CoFe_2O_4$ core–shell nanoparticle embedded P(VDF-TrFE) matrix. *Appl. Phys. Lett.* **2025**, *126*, 082903. [CrossRef]
42. Xie, S.H.; Ma, F.M.; Liu, Y.M.; Li, J.Y. Multiferroic $CoFe_2O_4$–$Pb(Zr_{0.52}Ti_{0.48})O_3$ Core–Shell Nanofibers and Their Magnetoelectric Coupling. *Nanoscale* **2011**, *3*, 3152–3158. [CrossRef] [PubMed]
43. Mushtaq, F.; Chen, X.; Torlakcik, H.; Steuer, C.; Hoop, M.; Siringil, E.C.; Marti, X.; Limburg, G.; Stipp, P.; Nelson, B.J.; et al. Magnetoelectrically Driven Catalytic Degradation of Organics. *Adv. Mater.* **2019**, *31*, 1901378. [CrossRef] [PubMed]
44. Urakova, A.; Baksheev, A.; Pryadko, A.; Grubova, I.; Surmeneva, M.; Chernozem, P.; Mukhortova, Y.; Wagner, D.; Gerasimov, E.; Kazantsev, S.; et al. Sub-20-nm Magnetite-Based Core–Shell Nanoparticles with Strong Magnetic, Magnetoelectric, and Nanocatalytic Properties. *Ceram. Int.* **2025**, *51*, 21702–21713. [CrossRef]
45. Mendes, M.C.; Martins, E.A.G.; Chernozem, R.V.; Chernozem, P.V.; Custódio, C.C.; Surmenev, R.A.; Kholkin, A.L.; Silva, A.S.; Mano, J.F. Osteogenic Differentiation Triggered by Intracellular Magnetoelectric Stimulation of Core–Shell Nanotransducers under Remotely Applied Magnetic Fields. *ACS Nano* **2025**, *19*, 42022–42045. [CrossRef] [PubMed]
46. Islam, R.A.; Bedekar, V.; Poudyal, N.; Liu, J.P.; Priya, S. Magnetoelectric Properties of Core–Shell Particulate Nanocomposites. *J. Appl. Phys.* **2008**, *104*, 104111. [CrossRef]
47. Cernea, M.; Radu, R.; Amorín, H.; Greculeasa, S.G.; Vasile, B.S.; Surdu, V.A.; Ganea, P.; Trusca, R.; Hattab, M.; Galassi, C. Lead-Free BNT–$BT_{0.08}$/$CoFe_2O_4$ Core–Shell Nanostructures with Potential Multifunctional Applications. *Nanomaterials* **2020**, *10*, 672. [CrossRef] [PubMed]
48. Yoo, K.; Jeon, B.G.; Chun, S.H.; Patil, D.R.; Lim, Y.-J.; Noh, S.-H.; Gil, J.; Cheon, J.; Kim, K.H. Quantitative Measurements of Size-Dependent Magnetoelectric Coupling in Fe_3O_4 Nanoparticles. *Nano Lett.* **2016**, *16*, 7408–7413. [CrossRef] [PubMed]
49. Betal, S.; Dutta, M.; Cotica, L.F.; Bhalla, A.S.; Guo, R. Control of crystalline characteristics of shell in core–shell magnetoelectric nanoparticles studied using HRTEM and holography. *Ferroelectrics* **2016**, *503*, 68–76. [CrossRef]
50. Chunduri, P.; Chanda, S.; Saha, S.; Gandhi, M.; Chinnaiah, S.; Rajesh, A. Structural Instability of $ZnFe_2O_4$–$BaTiO_3$ Magnetoelectric Core–Shell Nanoparticle: An In Situ Analysis by PFM. *J. Chin. Chem. Soc.* **2025**, *72*, 775–786. [CrossRef]
51. Bibani, M.; Breitwieser, R.; Aubert, A.; Loyau, V.; Mercone, S.; Ammar, S.; Mammeri, F. Tailoring the magnetic properties of cobalt ferrite nanoparticles using the polyol process. *Beilstein J. Nanotechnol.* **2019**, *10*, 1166–1176. [CrossRef] [PubMed]
52. Dhanyaprabha, K.C.; Jacob, B.; Mohan, M.; Al-Omari, I.A.; Al-Harthi, S.H.; Myint, M.T.Z.; Thomas, H. Magnetoelectric coupling study of lead-free $BaTiO_3$/$NiFe_2O_4$ mixed and core–shell multiferroic composites. *J. Mater. Sci. Mater. Electron.* **2023**, *34*, 207. [CrossRef]
53. Gulino, M.; Kim, D.; Tang, Q.; Sevim, S.; Zhang, E.; Ye, H.; Chen, X.-Z.; Morais, M.R.G.; Santos, S.D.; Pané, S.; et al. Magnetoelectric Core–Shell Nanoparticles for Nervous Tissue Electrostimulation: Performance in In Vitro and Ex Vivo Organotypic Cultures. *Acta Biomater.* **2026**, *209*, 504–520. [CrossRef] [PubMed]
54. Waters, M.; Hopf, J.; Tam, E.; Wallace, S.; Chang, J.; Bennett, Z.; Aquino, H.; Roeder, R.K.; Helquist, P.; Stack, M.S.; et al. Biocompatible, Multi-Mode, Fluorescent, T2 MRI Contrast Magnetoelectric-Silica Nanoparticles (MagSiNs), for On-Demand Doxorubicin Delivery to Metastatic Cancer Cells. *Pharmaceuticals* **2022**, *15*, 1216. [CrossRef] [PubMed]

55. Begines, B.; Ortiz, T.; Perez-Aranda, M.; Martinez, G.; Merinero, M.; Arguelles-Arias, F.; Alcudia, A. Polymeric Nanoparticles for Drug Delivery: Recent Developments and Future Prospects. *Nanomaterials* **2020**, *10*, 1403. [CrossRef] [PubMed]
56. Dang, Y.; Guan, J. Nanoparticle-Based Drug Delivery Systems for Cancer Therapy. *Smart Mater. Med.* **2020**, *1*, 10–19. [CrossRef] [PubMed]
57. Babic, M.; Horak, D.; Trchova, M.; Jendelova, P.; Glogarova, K.; Lesny, P.; Herynek, V.; Hajek, M.; Sykova, E. Poly(L-Lysine)-Modified Iron Oxide Nanoparticles for Stem Cell Labeling. *Bioconjugate Chem.* **2008**, *19*, 740–750. [CrossRef] [PubMed]
58. Dilnawaz, F.; Singh, A.; Mohanty, C.; Sahoo, S.K. Dual Drug Loaded Superparamagnetic Iron Oxide Nanoparticles for Targeted Cancer Therapy. *Biomaterials* **2010**, *31*, 3694–3706. [CrossRef] [PubMed]
59. Jain, T.K.; Morales, M.A.; Sahoo, S.K.; Leslie-Pelecky, D.L.; Labhasetwar, V. Iron Oxide Nanoparticles for Sustained Delivery of Anticancer Agents. *Mol. Pharm.* **2005**, *2*, 194–205. [CrossRef] [PubMed]
60. McCarthy, J.R.; Weissleder, R. Multifunctional Magnetic Nanoparticles for Targeted Imaging and Therapy. *Adv. Drug Deliv. Rev.* **2008**, *60*, 1241–1251. [CrossRef] [PubMed]
61. Yao, Y.; Zhou, Y.; Liu, L.; Xu, Y.; Chen, Q.; Wang, Y.; Wu, S.; Deng, Y.; Zhang, J.; Shao, A. Nanoparticle-Based Drug Delivery in Cancer Therapy and Its Role in Overcoming Drug Resistance. *Front. Mol. Biosci.* **2020**, *7*, 193. [CrossRef] [PubMed]
62. Stimphil, E.; Nagesetti, A.; Guduru, R.; Stewart, T.; Rodzinski, A.; Liang, P.; Khizroev, S. Physics considerations in targeted anticancer drug delivery by magnetoelectric nanoparticles. *Appl. Phys. Rev.* **2017**, *4*, 021101. [CrossRef]
63. Shotbolt, M.; Bryant, J.; Liang, P.; Khizroev, S. Physics of Selective Targeting of Cancer Cells by Magnetoelectric Nanoparticles: Exploring the Role of Conductivity and Capacitance in Tumor-Specific Attraction. *Adv. Theory Simul.* **2025**, *8*, e00739. [CrossRef]
64. Huang, R.; Lin, C.T.; Jiang, G.; Zhang, M.; Gao, W.; Aihemaiti, K.; Liu, Q.; Shi, J.; Shi, W.; Huang, R. BBB-penetrating magnetoelectric nanoparticles with sustainable Gel formulation for enhanced chemotherapy and reduced postoperative glioma recurrence. *Chem. Eng. J.* **2024**, *496*, 154208. [CrossRef]
65. Andre, M.; Kolishetti, N.; Yndart, A.; Vashist, A.; Nair, M.; Raymond, A.D. Magnetoelectric Extracellular Vesicle Latency-Targeting (MELT) Nanotherapeutic for the Block–Lock- and-Kill HIV Eradication Strategy. *Biomedicines* **2025**, *13*, 147. [CrossRef] [PubMed]
66. Song, J.; Liu, L.; Liu, Z.; Liu, S.; Zhang, Z.; Liu, X.; Heng, B.C.; Wang, Y.; Lu, D.; Zhang, X.; et al. Magnetoelectric nanoparticles drive TAF9B+ TH2 cell expansion to alleviate inflammation. *Sci. Adv.* **2026**, *12*, eadz3199. [CrossRef] [PubMed]
67. Zhang, J.; Shi, J.H.; Yang, Q.; Guo, H.; Guo, L.; Zhou, G.; Liu, Y.; Wang, X.; Hao, X.; Yang, Y. Nano-magnetoelectric biomimetic system promotes neural differentiation and reverses dopaminergic neuron damage for Parkinson's disease therapy. *Chem. Eng. J.* **2025**, *522*, 168308. [CrossRef]
68. Wang, P.; Toledo, D.; Zhang, E.; Telusma, M.; McDaniel, D.; Liang, P.; Khizroev, S. Scanning probe microscopy study of cobalt ferrite-barium titanate coreshell magnetoelectric nanoparticles. *J. Magn. Magn. Mater.* **2020**, *516*, 167329. [CrossRef]
69. Dembek, M.; Bocian, S.; Buszewski, B. Solvent Influence on Zeta Potential of Stationary Phase—Mobile Phase Interface. *Molecules* **2022**, *27*, 968. [CrossRef] [PubMed]
70. Martins, P.; Silva, M.; Lanceros-Mendez, S. Determination of the magnetostrictive response of nanoparticles via magnetoelectric measurements. *Nanoscale* **2015**, *7*, 9457–9461. [CrossRef] [PubMed]
71. Amiri, M.H.; Dehsari, H.S.; Asadi, K. Magnetoelectric coupling coefficient in multiferroic capacitors: Fact vs Artifacts. *J. Appl. Phys.* **2022**, *132*, 164102. [CrossRef]
72. Hossain, S.; Hossain, S. Magnetic and Optical Characterization of Cobalt Ferrite-Barium Titanate Core–Shell for Biomedical Applications. *IEEE Trans. Magn.* **2022**, *58*, 2501208. [CrossRef]
73. Hossain, S.; Hossain, S. Optical Characterization of Cobalt Ferrite and Magnetoelectric Cobalt Ferrite-Barium Titanate Core Shell Nanoparticles in Infra-Red Range. *IEEE Trans. Nanotechnol.* **2022**, *21*, 172–176. [CrossRef]
74. Wu, H.Y.; Vollmer, F. Coherent multipolar amplification of chiroptical scattering and absorption from a magnetoelectric nanoparticle. *Commun. Phys.* **2023**, *6*, 251. [CrossRef]
75. Llacer-Wintle, J.; Renz, J.; Hertle, L.; Veciana, A.; von Arx, D.; Wu, J.; Bruna, P.; Vukomanovic, M.; Puigmartí-Luis, J.; Nelson, B.J.; et al. The magnetopyroelectric effect: Heat-mediated magnetoelectricity in magnetic nanoparticle-ferroelectric polymer composites. *Mater. Horiz.* **2023**, *10*, 2627–2637. [CrossRef] [PubMed]
76. Zhang, E.; Shotbolt, M.; Abdel-Mottaleb, M.; Chen, S.; Andre, V.; Tian, J.; Shulgach, J.; Murphy, M.; Noga, B.; Liang, P.; et al. Magnetoelectric Nanoparticle-Based Wireless Brain–Computer Interface: Underlying Physics and Projected Technology Pathway. *Adv. Sci.* **2026**, e24329. [CrossRef] [PubMed]
77. Galletta, V.; Bonato, M.; Parazzini, M.; Chiaramello, E.; Fiocchi, S. In Silico analysis of concentration and spatial distribution effects of magnetoelectric nanoparticles on peripheral nerve activation. *Bioelectron. Med.* **2025**, *11*, 25. [CrossRef] [PubMed]
78. Bonato, M.; Galletta, V.; Zhang, E.; Cancino-Fuentes, N.; Chiaramello, E.; Fiocchi, S.; Sanchez-Vives, M.V.; Parazzini, M. In Silico Approach to Investigate Magnetoelectric Nanoparticle Effects for Minimally Invasive Brain Stimulation. In *Proceedings of the 47th Annual International Conference of the IEEE Engineering in Medicine and Biology Society (EMBC)*; IEEE: Piscataway, NJ, USA, 2025; pp. 1–4. [CrossRef] [PubMed]

79. Caiani, G.; Chiaramello, E.; Ravazzani, P.; Fiocchi, S. Resonant core–shell magnetoelectric nanoparticles as sensors of neural magnetic activity: A computational study. *Bioelectron. Med.* **2026**, *12*, 1. [CrossRef] [PubMed]
80. Lukat, N.; Friedrich, R.M.; Spetzler, B.; Kirchhof, C.; Arndt, C.; Thormählen, L.; Faupel, F.; Selhuber-Unkel, C. Mapping of magnetic nanoparticles and cells using thin film magnetoelectric sensors based on the delta-E effect. *Sens. Actuators A Phys.* **2020**, *309*, 112023. [CrossRef]
81. Huong Giang, D.T.; Dang, D.X.; Toan, N.X.; Tuan, N.V.; Phung, A.T.; Duc, N.H. Distance Magnetic Nanoparticle Detection Using a Magnetoelectric Sensor for Clinical Interventions. *Rev. Sci. Instrum.* **2017**, *88*, 015004. [CrossRef] [PubMed]
82. Friedrich, R.-M.; Sadeghi, M.; Faupel, F. Numerical and Experimental Study of Colored Magnetic Particle Mapping via Magnetoelectric Sensors. *Nanomaterials* **2023**, *13*, 347. [CrossRef] [PubMed]
83. Friedrich, R.-M.; Faupel, F. Adaptive Model for Magnetic Particle Mapping Using Magnetoelectric Sensors. *Sensors* **2022**, *22*, 894. [CrossRef] [PubMed]
84. Yadav, V.K.; Pathak, P.; Ganguly, P.; Mishra, P.; Das, S.; Mallick, D. Infrared-Driven Rapid Quantification of Magnetophoretically Trapped Drug. *J. Microelectromechanical Syst.* **2024**, *33*, 127–129. [CrossRef]
85. Mushtaq, S.; Shahzad, K.; Rizwan, M.; Ul-Hamid, A.; Abbasi, B.H.; Khalid, W.; Atif, M.; Ahmad, N.; Ali, Z.; Abbasi, R. Magnetoelectric core–shell $CoFe_2O_4$@$BaTiO_3$ nanorods: Their role in drug delivery and effect on multidrug resistance pump activity in vitro. *RSC Adv.* **2022**, *12*, 24958–24979. [CrossRef] [PubMed]
86. Rodzinski, A.; Guduru, R.; Liang, P.; Hadjikhani, A.; Stewart, T.; Stimphil, E.; Runowicz, C.; Cote, R.; Altman, N.; Datar, R.; et al. Targeted and Controlled Anticancer Drug Delivery and Release with Magnetoelectric Nanoparticles. *Sci. Rep.* **2016**, *6*, 20867. [CrossRef] [PubMed]
87. Mahdikia, H.; Saadati, F.; Alizadeh, A.M.; Khalighfard, S.; Bekeschus, S.; Shokri, B. Low-Frequency Magnetic Fields Potentiate Plasma-Modified Magneto-Electric Nanoparticle Drug Loading for Anticancer Activity In Vitro and In Vivo. *Sci. Rep.* **2023**, *13*, 17536. [CrossRef] [PubMed]
88. Guduru, R.; Khizroev, S. Magnetic Field-Controlled Release of Paclitaxel Drug from Functionalized Magnetoelectric Nanoparticles. *Part. Part. Syst. Charact.* **2014**, *31*, 605–611. [CrossRef]
89. Stewart, T.S.; Nagesetti, A.; Guduru, R.; Liang, P.; Stimphil, E.; Hadjikhani, A.; Salgueiro, L.; Horstmyer, J.; Cai, R.; Schally, A.; et al. Magnetoelectric Nanoparticles for Delivery of Antitumor Peptides into Glioblastoma Cells by Magnetic Fields. *Nanomedicine* **2018**, *13*, 423–438. [CrossRef] [PubMed]
90. Shahzad, K.; Mushtaq, S.; Rizwan, M.; Khalid, W.; Atif, M.; Din, F.U.; Ahmad, N.; Abbasi, R.; Ali, Z. Field-Controlled Magnetoelectric Core–Shell $CoFe_2O_4$@$BaTiO_3$ Nanoparticles as Effective Drug Carriers and Drug Release In Vitro. *Mater. Sci. Eng. C* **2021**, *119*, 111444. [CrossRef] [PubMed]
91. Hossain, S.; Guo, R.Y.; Bhalla, A. The Study of Core–Shell Cobalt Ferrite-Barium Titanate Magnetoelectric Nanoparticles in Targeting and Optimized Drug Delivery: An Overview. *Int. J. Nanosci.* **2024**, *23*, 2430001. [CrossRef]
92. Guduru, R.; Liang, P.; Hong, J.; Rodzinski, A.; Hadjikhani, A.; Horstmyer, J.; Levister, E.; Khizroev, S. Magnetoelectric Spin on Stimulating the Brain. *Nanomedicine* **2015**, *10*, 2051–2061. [CrossRef] [PubMed]
93. Kim, Y.J.; Kent, N.; Vargas Paniagua, E.; Driscoll, N.; Tabet, A.; Koehler, F.; Malkin, E.; Frey, E.; Manthey, M.; Sahasrabudhe, A.; et al. Magnetoelectric Nanodiscs Enable Wireless Transgene-Free Neuromodulation. *Nat. Nanotechnol.* **2025**, *20*, 121–131. [CrossRef] [PubMed]
94. Dominguez-Paredes, D.; Temel, Y.; Milojkovic, A.; Mulder-Jongen, D.; Kumari, P.; Ries, M.; Kozielski, K.; Jahanshahi, A. Magnetoelectric nanoparticle technology for mitigating motor deficits in Parkinsonian mice. *Brain Stimul.* **2025**, *18*, 1551–1560. [CrossRef] [PubMed]
95. Kozielski, K.L.; Jahanshahi, A.; Gilbert, H.B.; Yu, Y.; Francisco, D.; Alosaimi, F.; Temel, Y.; Sitti, M. Nonresonant Powering of Injectable Nanoelectrodes Enables Wireless Deep Brain Stimulation in Freely Moving Mice. *Sci. Adv.* **2021**, *7*, eabc4189. [CrossRef] [PubMed]
96. Singer, A.; Dutta, S.; Lewis, E.; Chen, Z.; Chen, J.C.; Verma, N.; Avants, B.; Feldman, A.K.; O'Malley, J.; Beierlein, M.; et al. Magnetoelectric Materials for Miniature, Wireless Neural Stimulation at Therapeutic Frequencies. *Neuron* **2020**, *107*, 631–643.e5. [CrossRef] [PubMed]
97. Choe, J.K.; Kim, S.; Lee, A.; Choi, C.; Cho, J.; Jo, W.; Song, M.H.; Cha, C.; Kim, J. Flexible, Biodegradable, and Wireless Magnetoelectric Paper for Simple In Situ Personalization of Bioelectric Implants. *Adv. Mater.* **2024**, *36*, e2311154. [CrossRef] [PubMed]
98. Murali, N.; Mukherjee, D.; Das, S.B.; Dhillon, A.K.; Siddhanta, S.; Mallick, D.; Betal, S. Magnetoelectric Core–Shell Nanoparticle-Based Wearable Hybrid Energy Harvesters for Biomedical Applications. *Adv. Eng. Mater.* **2023**, *25*, 2301061. [CrossRef]
99. Viteri, A.; Vargas-Estevez, C.; Colombi, S.; Resina, L.; Tan, H.; Sort, J.; Ginebra, M.-P.; Engel, E.; Alemán, C.; García-Torres, J. Three-Dimensional Magnetoelectric Nanocomposite GelMA Hydrogels for Wireless Electrical Stimulation of Cardiac Cells. *ACS Appl. Mater. Interfaces* **2026**, *18*, 28020–28032. [CrossRef] [PubMed]

100. Vinodan, K.; Balakrishnan, R.; Alias, S.; Sreelekshmi, N.; Thomas, N.G.; Raju, R.S.; Anil, S. Engineered Magnetoelectric PVDF-TrFE/$CoFe_2O_4$ Nanocomposite Fibers for Wound Healing Applications. *J. Drug Deliv. Sci. Technol.* **2026**, *124*, 108612. [CrossRef]
101. Ma, K.C.; Baumhauer, J.F. Pulsed Electromagnetic Field Treatment in Wound Healing. *Curr. Orthop. Pract.* **2013**, *24*, 487–492. [CrossRef]
102. Wu, M.; Rubin, A.E.; Dai, T.; Schloss, R.; Usta, O.B.; Golberg, A.; Yarmush, M. High-Voltage, Pulsed Electric Fields Eliminate Pseudomonas aeruginosa Stable Infection in a Mouse Burn Model. *Adv. Wound Care* **2021**, *10*, 477–489. [CrossRef] [PubMed]
103. Ju, H.W.; Lee, O.J.; Lee, J.M.; Moon, B.M.; Park, H.J.; Park, Y.R.; Lee, M.C.; Kim, S.H.; Chao, J.R.; Ki, C.S.; et al. Wound Healing Effect of Electrospun Silk Fibroin Nanomatrix in a Burn Model. *Int. J. Biol. Macromol.* **2016**, *85*, 29–39. [CrossRef] [PubMed]
104. Thao, N.T.T.; Wijerathna, H.M.S.M.; Kumar, R.S.; Choi, D.; Dananjaya, S.H.S.; Attanayake, A.P. Preparation and Characterization of Succinyl Chitosan and Succinyl Chitosan Nanoparticle Film: In Vitro and In Vivo Evaluation of Wound Healing Activity. *Int. J. Biol. Macromol.* **2021**, *193*, 1823–1834. [CrossRef] [PubMed]
105. Masson-Meyers, D.S.; Andrade, T.A.M.; Caetano, G.F.; Guimaraes, F.R.; Leite, M.N.; Leite, S.N.; Frade, M.A.C. Experimental Models and Methods for Cutaneous Wound Healing Assessment. *Int. J. Exp. Pathol.* **2020**, *101*, 21–37. [CrossRef] [PubMed]
106. Shotbolt, M.; Zhu, E.; Andre, V.; Zhang, E.; Duran, I.; Bryant, J.; El-Rifai, W.; Liang, P.; Khizroev, S. Catalytic Degradation of Organic Dyes Indicates Anti-Proliferative Effects of Magnetoelectric Nanoparticles. *J. Electron. Mater.* **2025**, *54*, 5529–5538. [CrossRef] [PubMed]
107. Shojaei Baghini, M.; Armada-Moreira, A.; Di Clemente, A.; Mukherjee, D.; Ofiare, A.; Harwell, J.; Dysko, M.; Benetti, L.; Bolster, D.; Maldonado, L.M.; et al. Bio-Integrated μBots with Overtone Ultrawideband Magnetoelectric Antennas for Wireless Telemetry. *Sci. Adv.* **2026**, *12*, eaec7011. [CrossRef] [PubMed]
108. Zaeimbashi, M.; Lin, H.; Dong, C.; Liang, X.; Nasrollahpour, M.; Chen, H.; Sun, N.; Matyushov, A.; He, Y.; Wang, X.; et al. NanoNeuroRFID: A Wireless Implantable Device Based on Magnetoelectric Antennas. *IEEE J. Electromagn. RF Microw. Med. Biol.* **2019**, *3*, 206–215. [CrossRef]
109. McGlynn, E.; Das, R.; Heidari, H. Encapsulated Magnetoelectric Composites for Wirelessly Powered Brain Implantable Devices. In Proceedings of the 27th IEEE International Conference on Electronics, Circuits and Systems (ICECS), Glasgow, UK, 23–25 November 2020; pp. 1–4. [CrossRef]
110. Truong, B.D.; Andersen, E.; Casados, C.; Roundy, S. Magnetoelectric Wireless Power Transfer for Biomedical Implants: Effects of Non-Uniform Magnetic Field, Alignment and Orientation. *Sens. Actuators A Phys.* **2020**, *316*, 112269. [CrossRef]
111. Nguyen, T.; Gao, J.; Wang, P.; Nagesetti, A.; Andrews, P.; Masood, S.; Vriesman, Z.; Liang, P.; Khizroev, S.; Jin, X. In Vivo Wireless Brain Stimulation via Non-Invasive and Targeted Delivery of Magnetoelectric Nanoparticles. *Neurotherapeutics* **2021**, *18*, 2091–2106. [CrossRef] [PubMed]

Disclaimer/Publisher's Note: The statements, opinions and data contained in all publications are solely those of the individual author(s) and contributor(s) and not of MDPI and/or the editor(s). MDPI and/or the editor(s) disclaim responsibility for any injury to people or property resulting from any ideas, methods, instructions or products referred to in the content.